phys. stat. sol. (b) **216**, 975 (1999)

Subject classification: 71.20.Nr; S5; S5.11; S5.12; S6; S7; S8

# Parameter Sets Due to Fittings of the Temperature Dependencies of Fundamental Bandgaps in Semiconductors

R. PÄSSLER[1])

*Institut für Physik, Technische Universität Chemnitz, D-09107 Chemnitz, Germany*

(Received June 22, 1999; in revised form July 30, 1999)

The temperature dependencies of the fundamental energy gaps of group-IV, III–V, and II–VI materials are fitted by means of a relatively simple analytical four-parameter expression. This is shown here to be capable of providing fine numerical fittings in combination with physically reasonable estimations of basic parameters. The majority of the materials under study are found to pertain to the regime of *intermediate* dispersion, where neither Varshni's formula nor the Bose-Einstein-related model function are capable of producing adequate fits. The effective phonon temperatures are estimated to amount as a rule to fractions of about 0.5 to 0.7 of the corresponding Debye temperatures. The availability of experimental $E(T)$ data up to the vicinity of the Debye temperature in a given material is found to be a necessary condition for trustworthy determinations of the limiting slopes of the $E(T)$ curves in the high-temperature region. This is achieved here for many materials by simultaneous fittings of fractional data sets owing to different authors and/or different experimental methods. The general cause of break-down of Varshni's formula, which has been noticed particularly in *wide* bandgap material studies, is clearly shown here by an inspection of higher-order derivatives to be due to its largely inadequate (ad hoc imputed) analytical form.

## 1. Introduction

There is large experimental evidence [1] for the fundamental bandgap widths, $E_g(T) = E_c(T) - E_v(T)$, of most group-IV, III–V, and II–VI semiconductor materials to decrease with increasing lattice temperature $T$. These $E_g(T)$ dependencies [1] are nonlinear at low as well as intermediate temperatures, $T \lesssim \Theta_D$ (= Debye temperature [1] of the material in question) and approach asymptotically to linear ones at sufficiently high temperatures, $T \gg \Theta_D$. The curvature of the nonlinear part of the $E_g(T)$ curve represents a material-specific "fingerprint", which is closely related to the actual position of the center of gravity, $\bar{\varepsilon}$, and the effective width (root-mean-square distance), $\Delta\varepsilon$, of the relevant spectrum of phonon modes that make substantial contributions to the observable $E_g(T)$ dependence. Depending on the ratio $\Delta\varepsilon/\bar{\varepsilon}$ between both basic features of the phonon energy spectrum we can distinguish the following (qualitatively different) dispersion regimes:

(1) Ratios $\Delta\varepsilon/\bar{\varepsilon} > 3^{-1/2} \approx 0.577$ correspond to the regime of *large* dispersion. This is realized in cases where the contribution of low-energy phonons (i.e. TA and long-wavelength LA phonons) is comparable with that of high-energy phonons (i.e. LO, TO, and short-wavelength LA phonons). The corresponding $E_g(T)$ dependencies show a *strong* curvature (tending to an apparently quadratic asymptote) in the cryogenic region and may be numerically simulated ("fitted") in *roughest* approximation by Varshni's formula [2, 3].

[1]) e-mail: paessler@physik.tu-chemnitz.de

(2) Ratios $\Delta\varepsilon/\bar{\varepsilon} \lesssim 1/3$ correspond to the regime of *small* dispersion. This tends to be realized in cases [4] where the contribution of low-energy phonons is very small in comparison with that of high-energy phonons. The corresponding $E_g(T)$ dependencies show a very *weak* dependence (tending to a plateau behavior) in the cryogenic region, and can be described in reasonable approximation by the familiar Bose-Einstein-related model function [4 to 6].

(3) However, for the majority of conventional semiconductor materials (in bulk), the dispersion ratios $\Delta\varepsilon/\bar{\varepsilon}$ can be found to lie fairly between $3^{-1}$ and $3^{-1/2}$, and their actual magnitude changes from material to material (see below). Thus we are concerned in practice predominantly with a regime of *intermediate* dispersion. Its adequate quantitative description requires more flexible analytical (four-parameter) representations [4, 7, 8]. Models of the latter type have been applied hitherto only to select semiconductor materials. It is the main aim of the present paper to present and to discuss in some detail the results of fittings of temperature dependencies of fundamental energy gaps, $E_g(T)$, and/or exciton peak energy positions, $E_{gx}(T)$, that are available from published literature for a larger variety of semiconductor materials.

## 2. Four-Parameter Model and Results of Numerical Fittings

Among the published analytical models which are suitable for fittings of $E_g(T)$ and/or $E_{gx}(T)$ dependencies pertaining to *different* dispersion regimes, the structurally simplest one is given by [7 to 9]

$$E(T) = E(0) - \frac{\alpha\Theta_p}{2}\left[\sqrt[p]{1+\left(\frac{2T}{\Theta_p}\right)^p} - 1\right]. \tag{1}$$

Here the parameter $\alpha \equiv S(\infty)$ represents the $T \to \infty$ limiting magnitude of the slope (= entropy [3, 7]),

$$S(T) \equiv -\frac{\mathrm{d}E(T)}{\mathrm{d}T}, \tag{2}$$

of the $E(T)$ curve in question, and $\Theta_p$ is approximately equal to the average phonon temperature, $\Theta_p \approx \Theta \equiv \bar{\varepsilon}/k_B$ (= eq. (9) in [8]; for more details see below). Referring to basic model relations (given in Sec. 3 of Ref. [8]) one can see that the fractional exponent $p$ in (1) is connected with the material-specific degree of phonon dispersion, $\Delta\varepsilon/\bar{\varepsilon}$, by the approximate relation

$$\frac{\Delta\varepsilon}{\bar{\varepsilon}} \approx \frac{1}{\sqrt{p^2-1}}, \quad \text{i.e. conversely} \quad p \approx \sqrt{1+\left(\frac{\Delta\varepsilon}{\bar{\varepsilon}}\right)^{-2}}. \tag{3}$$

This means that the regimes of large and small dispersion are approximately represented within this model by exponents $p < 2$ and $p \gtrsim 3.3$, respectively.

We have fitted experimental $E_g(T)$ and/or $E_{gx}(T)$ data sets for a variety of group IV, III–V, and II–VI semiconductor materials by means of eq. (1) (details are discussed below). The numerical values resulting from these fitting for the parameters $p$, $\alpha$, and $\Theta_p$ (in combination with fitted $E_g(0)$ and/or $E_{gx}(0)$ values) are listed in Table 1.

Table 1

Empirical parameter values resulting from numerical fittings of experimental $E_g(T)$ (fundamental bandgap) and/or $E_{gx}(T)$ (exciton peak) data available for various group-IV, III–V, and II–VI materials. The $T \to 0$ limiting values for the fundamental bandgap energies, $E_g(0)$ (listed in the forth column), are given by the sum $E_{gx}(0) + E_{bx}$ of the corresponding exciton gap energy, $E_{gx}(0)$, and exciton binding energy, $E_{bx}$ [1]. (Note that the magnitude of the latter is unknown hitherto in the cases of 15R SiC [11, 12], AlP [17], and AlAs [18].)

| | $E(T)$ data (Ref.) | $T_{fitted}$ (K) | $E_g(0)$ (eV) | $p$ | $\alpha$ (meV/K) | $\Theta_p$ (K) | $\Theta_D$ (K) | $\Theta_p/\Theta_D$ | $\Delta\varepsilon/\bar{\varepsilon}$ |
|---|---|---|---|---|---|---|---|---|---|
| C | [10] | 103 to 660 | 5.49 | 3.3 (fixed) | (0.50) | (1067) | 1860 | (0.57) | (0.32) |
| 15R SiC | [11, 12] | 6 to 645 | $2.986 + E_{bx}$ | 3.08 | 0.417 | 669 | 1200 | 0.56 | 0.34 |
| Si | [13, 14] | 2 to 415 | 1.170 | 2.33 | 0.318 | 406 | 674 | 0.60 | 0.48 |
| Ge | [15] | 4 to 416 | 0.744 | 2.38 | 0.407 | 230 | 374 | 0.61 | 0.46 |
| AlN | [16] | 4 to 298 | 6.20 | 3.0 (fixed) | (0.83) | (575) | 950 | (0.61) | (0.35) |
| AlP | [17] | 8 to 302 | $2.49 + E_{bx}$ | 2.5 (fixed) | (0.35) | (130) | 588 | (0.22) | – |
| AlAs | [18] | 4 to 287 | $2.229 + E_{bx}$ | 2.32 | 0.362 | 218 | 417 | 0.52 | 0.48 |
| AlSb | [19] | 4 to 298 | 1.686 | 1.90 | 0.343 | 226 | 380 | 0.59 | 0.62 |
| GaN | [20] | 2 to 1067 | 3.47 | 2.62 | 0.599 | 504 | 870 | 0.58 | 0.41 |
| GaP | [21, 22] | 4 to 680 | (2.339) | 2.09 | 0.480 | 358 | 500 | 0.72 | 0.55 |
| GaAs | [23, 24] | 2 to 673 | 1.519 | 2.44 | 0.472 | 230 | 360 | 0.64 | 0.45 |
| GaSb | [25] | 9 to 300 | 0.811 | 2.57 | 0.375 | 176 | 266 | 0.50 | 0.42 |
| InN | [26] | 4 to 300 | 1.994 | (2.9) | (0.21) | (453) | (700) | – | (0.37) |
| InP | [27, 28] | 4 to 873 | 1.424 | 2.51 | 0.391 | 243 | 420 | 0.58 | 0.43 |
| InAs | [29] | 10 to 300 | 0.414 | 2.10 | 0.281 | 143 | 262 | 0.55 | 0.54 |
| InSb | [29, 30] | 10 to 550 | 0.234 | 2.68 | 0.250 | 136 | 205 | 0.53 | 0.40 |
| ZnS | [31] | 2 to 541 | 3.841 | 2.76 | 0.532 | 240 | 440 | 0.55 | 0.39 |
| ZnSe | [31, 32] | 4 to 500 | 2.825 | 2.67 | 0.490 | 190 | 340 | 0.56 | 0.40 |
| ZnTe | [31] | 2 to 291 | 2.394 | 2.71 | 0.454 | 145 | 260 | 0.56 | 0.40 |
| CdS | [33/36] | 2 to 289 | 2.583 | 2.47 | 0.402 | 147 | 280 | 0.53 | 0.44 |
| CdSe | [37] | 15 to 550 | 1.846 | 2.58 | 0.405 | 168 | 300 | 0.56 | 0.42 |
| CdTe | [38] | 2 to 300 | 1.606 | 1.97 | 0.310 | 108 | 160 | 0.68 | 0.59 |

## 3. Discussion

Viewing the estimated $p$ values (or the corresponding $\Delta\varepsilon/\bar{\varepsilon}$ ratios (3)) listed in Table 1 we see, first of all, that the limiting regimes of large or small dispersion are realized only in few cases, namely: the data available for AlSb [19] and CdTe [38] are indicative of large dispersion whereas the data for diamond [10] seem to be indicative for small dispersion. All other $p$ values fall into the interval between 2.0 and 3.3, which pertains to the regime of intermediate dispersion.

Assessing further the $T \to \infty$ limits of the slopes, $\alpha \equiv S(\infty)$, we see from Table 1 that, except for AlN and InN, their magnitudes are ranging within the relatively narrow interval of about $3 \times 10^{-4}$ eV/K $< \alpha < 6 \times 10^{-4}$ eV/K. This is a physically rather important result especially in view of a series of inadequate $\alpha$ values (such as $17 \times 10^{-4}$ eV/K for ZnS and CdSe [39, 40]), which have been obtained by earlier fittings using Varshni's formula [2, 3],

$$E_{Var.}(T) = E(0) - \frac{\alpha_{Var.} T^2}{\beta + T} \,. \tag{4}$$

Moreover we see from Table 1 that, except for AlP [17] (cf. also [41]), the ratios $\Theta_p/\Theta_D$ between the estimated phonon temperatures, $\Theta_p$, and the associated Debye temperatures [1], $\Theta_D$, are ranging within the physically reasonable interval of $0.5 < \Theta_p/\Theta_D < 0.7$, i.e. the centers of gravity of the relevant electron–phonon interaction are located as a rule *within* the *upper* half (slightly above the middle) of the relevant phonon spectra. At the same time we would like to point out that, due to the relative simplicity (approximate nature) of eq. (1) [4, 8], an empirical $\Theta_p$ value is not precisely coinciding with the actual magnitude of the average phonon temperature, $\Theta \equiv \bar{\varepsilon}/k_B$ [8], for a given material. Deviations between $\Theta_p$ and $\Theta$ are vanishing in the vicinity of $p \approx 2$ (i.e. in the transition region between large and intermediate dispersion), but they are increasing up to an order of 20% in the vicinity of $p \approx 3$ (i.e. in the transition region between intermediate and small dispersion). The magnitudes of both parameters follow from more detailed numerical analyses to be connected by the approximate relationship

$$\Theta \approx \Theta_p \, (1.152 + 0.145 \ln (p - 1.7)) \, . \tag{5}$$

Nevertheless, for many practical purposes it does not appear inadequate (at the present stage of investigations, at least) to use still a relatively simple four-parameter formula like eq. (1). The knowledge of the corresponding empirical parameter set ($\alpha$, $\Theta_p$, $p$, and $E(0)$), as resulting from a least-mean-square fit of a given $E(T)$ curve by eq. (1), enables a subsequent calculation of the whole $E(T)$ dependence including, if necessary, an extrapolation far beyond the experimentally covered range. It is important to bear in mind, however, that such extrapolations can be considered as trustworthy only in cases where the experimental $E(T)$ data set comprises a temperature range up to the vicinity (or even slightly beyond [31]) the effective Debye temperature, $\Theta_D$ [1]. (Note that it follows from basic relations of the theory [8] that the magnitudes of the slopes, $S(T)$ (eq. (2)), which are detectable at the upper ends of measured $E(T)$ curves, are closely approaching their limiting magnitudes, $S(\infty) \equiv \alpha$, only at $T \gtrsim \Theta_D$.) If, in contrast to this, the experimental measurements have been broken off at a temperature much lower than $\Theta_D$, the limiting slope can be estimated only to within relatively large error bars (of the order of 5% to 20%). Consequently, due to the usually rather strong interdependence between all empirical parameters, the fitted parameter set remains as a whole relatively uncertain. (Such parameter sets have been enclosed into brackets in Table 1.) Let us briefly discuss characteristic features of the numerical results obtained by our fittings of the individual $E_g(T)$ and/or $E_{gx}(T)$ data sets in consideration.

### *3.1 Analyses and results for group-IV materials*

Various numerical problems and uncertainties which we have frequently to face in numerical analysis of more or less deficient $E(T)$ data sets can be well exemplified by considering the indirect exciton gap data given by Clark et al. [10] for ***diamond*** (see Fig. 1), namely:

(i) The break-off temperature for the measurements (of about 660 K) amounts to only about 35% of the corresponding Debye temperature (cf. Table 1). Thus, in view of the theoretical arguments given above, the value obtained for the limiting slope, $\alpha$, can hardly be considered as a definitive one.

(ii) The complete lack of experimental $E_{gx}(T)$ data for low temperatures, $T < 100$ K, involves an uncertainty of several meV with respect to the $T \to 0$ exciton gap,

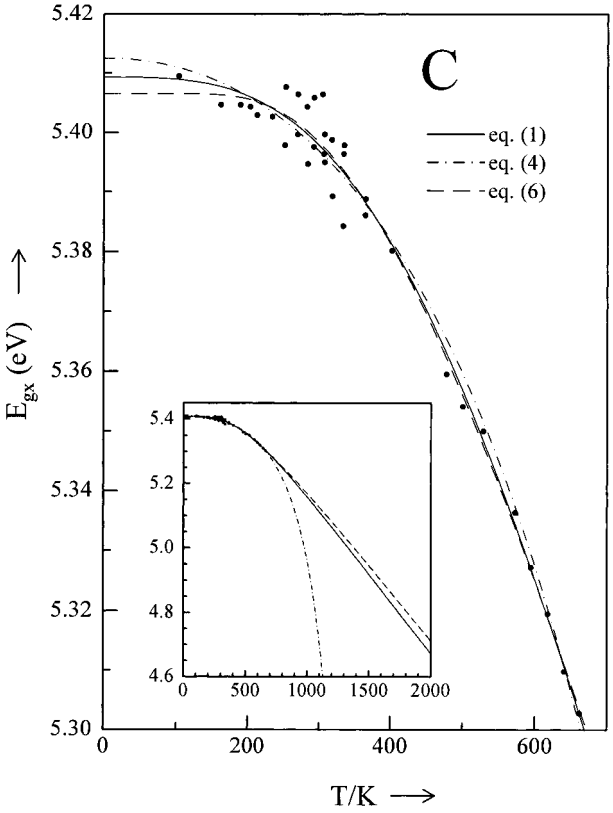


Fig. 1. Fittings of the exciton energy gap data given for diamond by Clark et al. [10]

$E_{gx}(0) = 5.409$ ($\pm 0.003$) eV. (Combining the latter with an exciton binding energy of $E_{bx} = 0.07$ eV [1] one can roughly estimate the $T \to 0$ value of the indirect band gap energy to be $E_g(0) \approx 5.48$ eV [1].)

(iii) The relatively large error bars (up to $\pm 10$ meV) between 200 and 350 K reduce considerably the reliability of estimates of the remaining parameters $\Theta_p$ and $p$. In view of these unusually large experimental uncertainties for diamond, it appeared adequate to fix in this case the parameter $p$ (in analogy to the cases of AlN and AlP; cf. Table 1).

Yet, despite of all these uncertainties, it appears from Fig. 1 that the fit by eq. (1) gives a reasonable description of the measured behavior within the interval between 350 and 660 K (at least). Furthermore it is instructive to note that another fit, which is at $T > 200$ K almost indistinguishable from the former one, follows from the model of Bose-Einstein type [4 to 6],

$$E_{B.-E.}(T) = E(0) - \frac{\alpha\Theta}{\exp\left(\frac{\Theta}{T}\right) - 1} \equiv E(0) - \frac{\alpha\Theta}{2}\left(\coth\left(\frac{\Theta}{2T}\right) - 1\right). \tag{6}$$

The corresponding empirical parameter values are $E_{gx}(0) = 5.407$ eV, $\alpha = 0.490$ meV/K, and $\Theta = 1308$ K. From Table 1 we see that the latter $E_{gx}(0)$ and $\alpha$ values are by only 0.002 eV and 0.010 meV/K lower than their counterparts due to eq. (1) and the associated phonon temperature values are in reasonable agreement with the empirical relation (5) between $\Theta$ and $\Theta_p$ (for $p = 3.3$). The alternative descriptions of the measured

$E_{gx}(T)$ dependencies by eqs. (1) and (6) are thus found to be nearly equivalent so that a qualitative discrimination between both models can not be made, in this particular case. In contrast to these physically reasonable interpretations basing on eqs. (1) and (6), Varshni's attempt [2] to fit the same data set by eq. (4) has led to *negative* values both for $\alpha_{Var.}$ and $\beta$ (namely $\alpha_{Var.} = -0.1979$ meV/K and $\beta = -1437$ K, in combination with $E_{gx}(0) = 5.4125$ eV [2]; the corresponding $E_{Var.}(T)$ dependence is represented by the dash-dotted curve in Fig. 1). We have compared in the inset to Fig. 1 all three calculated curves up to the vicinity of the Debye temperature. We see that, even at such high temperatures, the difference between the alternative curves due to eqs. (1) and (6) is still moderate (being of an order of only 0.03 eV). In contrast to this, the $E_{Var.}(T)$ curve [2] drops dramatically with increasing temperature. This excessively strong drop of the $E_{Var.}(T > 660$ K) curve is followed even by a *singularity*, $E_{Var.}(T \to |\beta|) \to \pm\infty$, which is emerging when $T$ in eq. (4) approaches the singular point $|\beta| = -\beta = 1437$ K [2]. Peculiarities of this type due to eq. (4) are computational artifacts which have nothing to do with physical reality. Such a singularity in an $E(T)$ curve has never been observed experimentally (neither in diamond nor in any other material). Moreover, the generally accepted basic equations describing $E_g(T)$ dependencies in semiconductors (see [8] and papers cited therein) give no space for the emergence of a singularity, whichever the actual form of the electron–phonon spectral function would be. Consequently, Varshni's numerical simulation (pseudo-fit) of the $E_{gx}(T)$ dependence for diamond must be strictly rejected from physical points of view. (More insight into the causes of the frequently encountered incapability of Varshni's formula of producing satisfactory least-square fits with physically reasonable parameter values will be given in Sections 4 and 5).

A rather accurate and quantitatively very informative $E_{gx}(T)$ data set was given by Patrick et al. [11] for the 15R polytype of ***silicon carbide*** (SiC). An excellent fit of these data (see Fig. 2), which is characterized by an unusually low variance (of only 0.3 meV$^2$), is due to eq. (1). Another physically reasonable fit can be produced again by eq. (6). Due to the notorious plateau behavior of eq. (6) in the cryogenic region, however, this change to the simpler analytical model (6) is connected with a significant increase of the variance (up to about 1.3 meV$^2$). The corresponding empirical parameter values are $E_{gx}(0) = 2.985$ eV, $\alpha = 0.429$ meV/K, and $\Theta = 804$ K. In analogy to the parameter constellations for diamond we find thus also for the case of 15R SiC that the latter $E_{gx}(0)$ and $\alpha$ values are by only 0.001 eV and 0.012 meV/K lower than their counterparts due to eq. (1) (listed in Table 1). Rather instructive is an alternative fit by Varshni's formula (eq. (4)). In this case the variance raises up to about 5.9 meV$^2$. This indicates already a significant (order-of-magnitude) deterioration of the fit in comparison with eq. (1) (cf. the inset to Fig. 2). Much more dramatic than the corresponding misfit in the cryogenic region, however, is the inherent order-of-magnitude increase of Varshni's parameter values as resulting from the least-square fitting process. The fully relaxed parameter values are $\alpha_{Var.} = 17.5$ meV/K and $\beta = 50098$ K. Such a floating ("inflation") of Varshni's parameter set over *several orders of magnitude*, in the case of 15R SiC, is another characteristic exemplification of the repeatedly noticed break-down of Varshni's formula (see Section 5).

For various practical applications it would be desirable to dispose of similar parameter sets for more common SiC polytypes like 3C, 4H, and 6H. Unfortunately, $E_{gx}(T)$ data sets which would be similarly informative as in the case of 15R [11] are not avail-

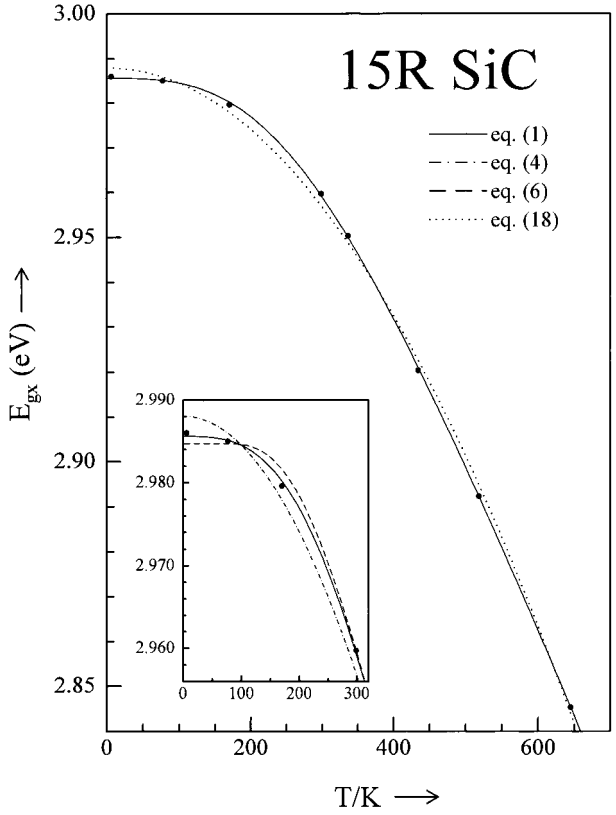


Fig. 2. Fittings of the exciton energy gap data given for 15R silicon carbide by Patrick et al. [11]

able hitherto for these polytypes. From purely numerical points of view, the $E_{gx}(T < 200\,\mathrm{K})$ data sets given for 4H SiC by Choyke et al. [42] and for 6H SiC by Choyke and Patrick [43] can again be perfectly fitted using eq. (1). However, in view of the circumstance that the experimental break-off temperature (of about 200 K) is by a factor of about six lower than the corresponding Debye temperature, $\Theta_D \approx 1200$ K, one can hardly expect to come in this way to a trustworthy determination of parameter sets. However, one can see e. g. from Fig. 2 in Ref. [44] that, for a large variety of SiC polytypes, the $E_{gx}(T)$ dependencies behave quite similarly (up to 800 K, at least) as the $E_{gx}(T)$ dependence for 15R (Fig. 2). Consequently one can use in good approximation the parameter values $\alpha$, $\Theta_p$, and $p$ given in Table 1 also for a calculation of the temperature dependence of $E_{gx}(T)$ or $E_g(T)$ in other polytypes. To this end it is but necessary to insert into eq. (1) proper values for the structure-specific $T \to 0$ gap energies, $E_{gx}(0)$ or $E_g(0)$ (some of which are given in Refs. [1] and [44]).

Less problematic is the numerical analysis of $E_{gx}(T)$ or $E_g(T)$ dependencies shown by the conventional group-IV semiconductor materials silicon and germanium. In Fig. 3 we have plotted the detailed $E_g(T)$ data set given for ***silicon*** (Si) by Bludau et al. [13]. The relatively high density of experimental points in this case enables above all a trustworthy determination of the dispersion ratio, $\Delta\varepsilon/\bar{\varepsilon}$ (3), via the fractional exponent $p$. At the same time we see that the experimentally chosen break-off temperature (of 300 K)

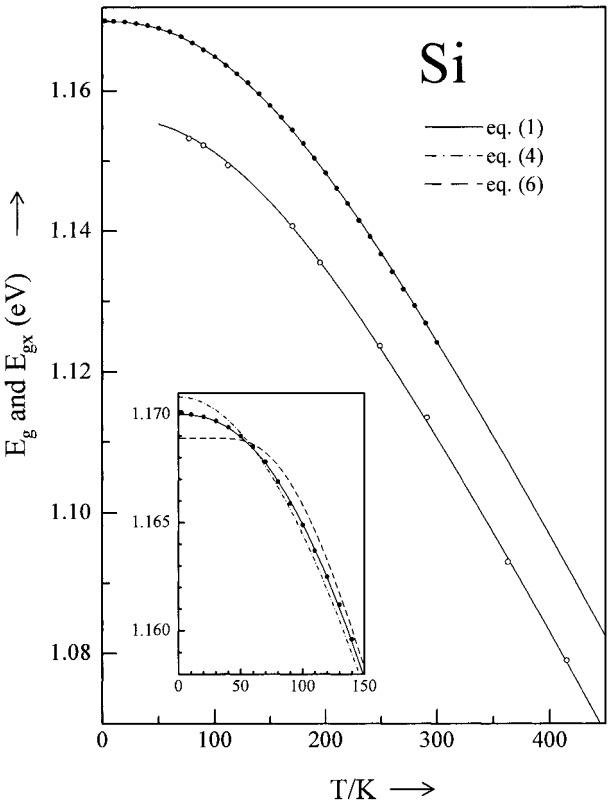


Fig. 3. Simultaneous fittings of the fundamental bandgap energy data given for silicon by Bludau et al. [13] (filled circles) in combination with exciton energy gap data due to Macfarlane et al. [14] (empty circles)

is by a factor of about two lower than the associated Debye temperature (cf. Table 1). Some additional information on the temperature dependence *beyond* room temperature is therefore useful for a trustworthy determination of the limiting slope, $\alpha \equiv S(\infty)$. Accordingly we have taken into consideration the exciton energy gap values, $E_{gx}(T)$, given for Si by Macfarlane et al. [14]. The simultaneous fitting of both experimental curves using eq. (1) leads to the values listed in Table 1 (for $\alpha$, $\Theta_p$, and $p$) in combination with the zero-temperature energy positions $E_{gx}(0) = 1.156$ eV and $E_g(0) = 1.170$ for the lower and upper curve, respectively. From the inset to Fig. 3 we see that eq. (1) provides a very fine fit of the measured $E_g(T)$ dependence [13] even in the cryogenic region. In contrast to this, the curves following from fittings by eqs. (4) or (6) show systematic deviations from the observed behavior. The comparison of all three curves shows that the behavior of the $E_g(T)$ curve due to eq. (1) is somehow intermediate between the extremes of a very strong curvature (due to eq. (4)), on the one hand, and a $T \to 0$ plateau behavior (due to eq. (6)), on the other hand. Such an alternative curve constellation is typical for the majority of the materials in question (see below). This picture is consistent with a dispersion ratio of $\Delta\varepsilon/\bar{\varepsilon} = 0.48$ (see Table 1), which is ranging fairly in the middle region between the limiting regimes of large ($\Delta\varepsilon/\bar{\varepsilon} > 0.57$) and small ($\Delta\varepsilon/\bar{\varepsilon} < 0.33$) dispersion.

Much scarcer are the experimental data for ***germanium*** (Ge). We have plotted in Fig. 4 the set of exciton energy gap values, $E_{gx}(T)$, which had been given for Ge by

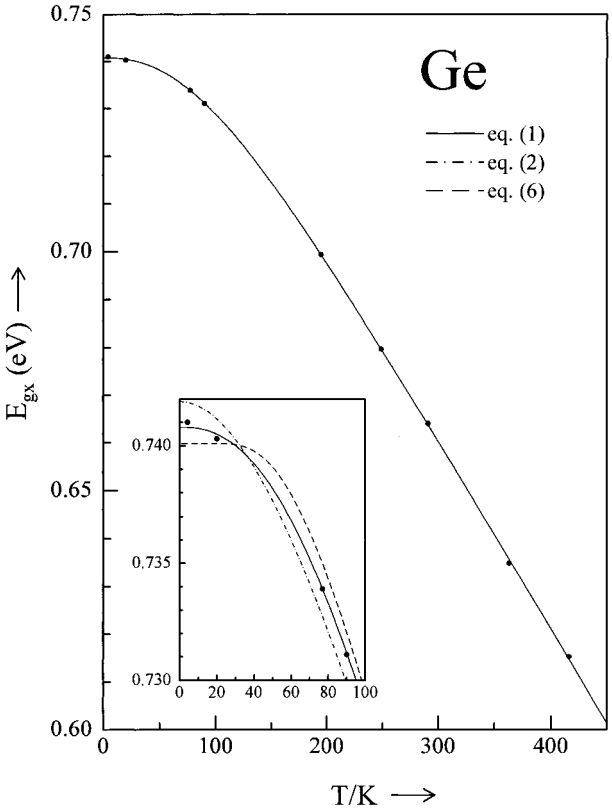


Fig. 4. Fittings of the exciton energy gap data given for germanium by Macfarlane et al. [15]

Macfarlane et al. [15]. In contrast to the case of silicon, the experimentally chosen break-off temperature (of 416 K [15]) for germanium lies *above* the corresponding Debye temperature (cf. Table 1). Thus the $E_{gx}(T)$ data set in question should be sufficient for a proper determination of the limiting slope, $\alpha \equiv S(\infty)$. Moreover, the fit obtained using eq. (1) is characterized by an unusually low variance (of only 0.22 meV$^2$). Thus there are good reasons to suppose that, despite of the relative scarcity of this data set, the resulting parameter values are adequate. Combining the $T \to 0$ limit of the excitonic gap, $E_{gx}(0) = 0.741$ eV (see Fig. 4), with the known exciton binding energy, $E_{bx}(0) = 2.7$ meV [1], one comes to the known value of $E_g(0) = 0.744$ eV [1] for the $T \to 0$ limit of the fundamental energy gap (cf. Table 1). From Table 1 we see, among other things, that the magnitudes of $p$ and, consequently, also the dispersion ratios, $\Delta\varepsilon/\bar{\varepsilon}$, are nearly the *same* in Ge and Si. This means an approximate equality of the normalized (dimensionless) representations, $\eta_p(\xi)$ [8], of both curves (for more detail see Section 4).

### *3.2 Analyses and results for III–V compounds*

Let us consider first the aluminum group-V compounds. The $E(T)$ data sets which we could find in literature for these materials, all are ending in the vicinity of room temperature whereas the Debye temperatures are relatively high (ranging between 380 and 950 K; cf. Table 1). In addition to this, some of these data sets are very scarce. Thus the

parameter values obtained for these four materials can be considered only as provisional ones.

This applies in particular to ***aluminum nitride*** (AlN). Fig. 5 shows the $E(T \leq 298\ \mathrm{K})$ data set given for AlN by Brunner et al. [16]. In view of the lack of experimental data for higher temperatures we have performed the fitting by eq. (1) at fixed $p = 3.0$ (cf. Table 1). The quality of this fit is characterized by a relatively low variance (of only 0.57 $\mathrm{meV}^2$). This suggests that eq. (1) should be applicable also to ternary materials like $Al_xGa_{1-x}N$ [16] (having bandgap energies up to an order of 6 eV). At the same time, the low variance of our fit can be taken as an indication of an obviously high degree of accuracy (internal consistency) of the $E(T \leq 298\ \mathrm{K})$ data set due to Brunner et al. [16] (especially in comparison with an earlier $E(T \leq 298\ \mathrm{K})$ data set given for AlN by Guo and Yoshida [26], whose variance amounts to about 30 $\mathrm{meV}^2$). From an alternative fit of the $E(T \leq 298\ \mathrm{K})$ data set due Brunner et al. [16] by the Bose-Einstein-related model (eq. (6)) we have obtained the parameter values of about $\alpha = 0.66$ meV/K and $\Theta = 560$ K (with a residual variance of about 1.6 $\mathrm{meV}^2$). The latter value for $\alpha$ is by about 20% lower than that resulting from eq. (1) (cf. Table 1). Which of both might be more correct can by no means decided on the basis of the data sets presently available for AlN. This comparison illustrated ones more the great importance of extending experimental measurements in *wide* bandgap materials *far beyond room temperature.*

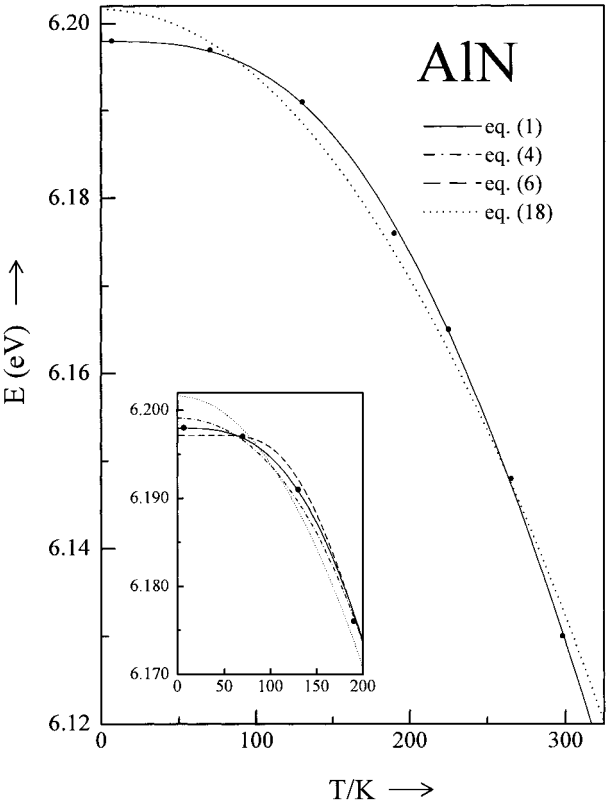


Fig. 5. Fittings of the bandgap energy data given for aluminum nitride by Brunner et al. [16]

Much less informative is the $E_{gx}(T)$ data set available for ***aluminum phosphide*** (AlP) from Ref. [17]. This data set consists not only of very few experimental points (namely seven, in analogy to AlN) but, in addition to this scarcity, these data points are obviously also rather inaccurate. This can be concluded from the fact that fittings of these data lead throughout to unusually large values for variances (being larger than 10 meV$^2$, for *all* analytical models in consideration). We believe that the relatively large experimental error bars (of about $\pm$10 meV [17]) are the reason for the unusually small magnitude obtained here (in analogy to [41]) for the ratio $\Theta_p/\Theta_D$. (Note that an apparent ratio of $\Theta_p/\Theta_D \approx 0.22$, for AlP, is by factors two to three smaller than those for *all* other materials in question; cf. Table 1. Such a small $\Theta_p/\Theta_D$ ratio would correspond to an anomaly, where the $E_g(T)$ dependence would be produced almost exclusively by low-energy phonons.) Possible future measurements of $E_g(T)$ or $E_{gx}(T)$ dependencies for AlP are likely to lead to a largely different parameter constellation.

More informative data are given by Monemar [17] on temperature dependencies of threshold energies for various phonon assisted indirect transitions in ***aluminum arsenide*** (AlAs). By fitting the whole data set (Fig. 3 in [18]) by a unique set of basic parameters, in combination with properly adjusted $E(0)$ positions for the individual phonon assisted transitions, we have obtained the $\alpha$, $\Theta$, and $p$ values listed in Table 1.

A series of temperature dependencies for the energies of phonon assisted indirect transitions in ***aluminum antimonide*** (AlSb) are given by Alibert et al. [19]. The individual series of experimental points are partly very scarce so that some rough estimation of basic parameters could be made only by a simultaneous fitting of all these data (in analogy to AlAs). The perhaps most interesting result of this fit consists in a $p$ value *lower* than two. This is indicative, according to eq. (3), for the regime of large dispersion, $\Delta\varepsilon/\bar{\varepsilon} > 0.57$, which was found to be realized only in few cases (cf. Table 1). This assignment can be confirmed by considering a certain $E_g(T)$ data set given for AlSb by Sirota at al. [45], whose fitting leads equally to a $p$ value *lower* than two. Consequently, in this particular case, a relatively good fit can be produced also by Varshni's formula. The curves resulting from alternative fittings of the whole data set by eqs. (1) and (4) turned out to be practically indistinguishable.

Much more comprehensive and informative $E_g(T)$ and/or $E_{gx}(T)$ data sets than in cases of aluminum group-V compounds are available for gallium group-V compounds. Consider first the case of the technologically very important wide bandgap material ***gallium nitride*** (GaN). A larger series of papers on temperature dependencies of excitonic and other near bandgap emission and absorption features both for GaN bulk samples and layers (with both hexagonal and cubic structure, due to different substrates) have been published in last years. Unfortunately, the overwhelming majority of these experimental studies was restricted to a range from cryogenic up to *room* temperature. The Debye temperature in GaN is, in analogy to all other semiconductor materials in question, an inherently temperature-dependent quantity [1]. From Ref. [46] we see that the Debye temperature raises in hexagonal GaN from the usually quoted *low*-temperature value of $\Theta_D(T \rightarrow 0) \approx 600$ K [1] up to an effective *high*-temperature value of $\Theta_D(T > 300\ \text{K}) \approx 870$ K [46] (cf. Table 1; note that it is always the latter limit of $\Theta_D$ which is to be referred to in order-of-magnitude comparisons with effective phonon temperatures obtained by numerical analyses of $E(T)$ dependencies). In view of this high Debye temperature it is clear that for GaN (in analogy to AlN) such restricted $E(T \leq 300\ \text{K})$ data sets are largely insufficient for a trustworthy determination

of the empirical parameter set (which analytical model would ever be used for such an estimation). Fortunately, several groups of investigators have already published results of measurements for hexagonal GaN layers far *beyond* room temperature (see in particular Teisseyre et al. [47] and Zubrilov et al. [48]). An especially informative $E(T)$ data set, which comprises an unusually large temperature range (from 2 K up to 1067 K) has been presented by Herr [20] (see Fig. 6). Assessing the parameter values (given in Table 1) for the fit by eq. (1) it may be important to note that the order of $\alpha \approx 0.6$ meV/K, for the high-temperature limit of the slope, follows not only from the analysis of Herr's data set [20] (Fig. 6). Nearly the same magnitude for $\alpha$ follows also from analogous fittings (by eq. (1)) of the data sets given by Teisseyre et al. [48] and Zubrilov et al. [49]. This approximate equality of $\alpha$ values due to different authors suggests that an order of 0.6 meV/K might be typical for the limiting slope in *hexagonal* GaN layers. In contrast to this, fittings of a large series of *restricted* $E(T \lesssim 300$ K) data sets, which have been published in recent years for hexagonal GaN layers, lead in many cases to markedly different $\alpha$ values (ranging between about 0.3 and 0.8 meV/K; such parameter uncertainties for GaN illustrate once more the necessity of performing measurements for *wide* bandgap materials far *beyond* room temperature). The present estimation of $\Theta_p/\Theta_D = 0.58$, for the ratio between $\Theta_p$ (= 504 K) and $\Theta_D$ (= 870 K) in hexagonal GaN, is in accordance with the common trend (cf. Table 1). If we had estimated this ratio by referring to the more familiar value of 600 K [1] for the Debye

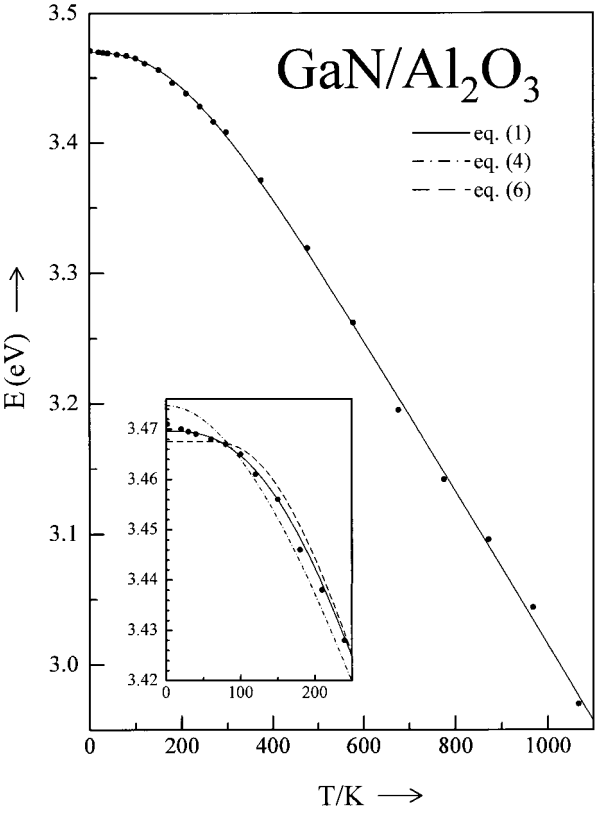


Fig. 6. Fittings of the of the bandgap energy data given for gallium nitride by Herr [20]

temperature, we would have obtained a ratio $>0.8$. The latter would lie clearly outside the typical range (of 0.5 to 0.7, cf. Table 1). This observation gives a further hint that the relevant (i.e. high-temperature limiting) value of the Debye temperature in GaN should actually be significantly higher than 600 K (in accordance with the theoretical results presented in Ref. [46]). Further we would like to point out that a dispersion ratio of about 0.4 for the hexagonal GaN layer in question [26] falls into the *lower* part ($0.33 \leq \Delta\varepsilon/\bar{\varepsilon} \leq 0.45$) of the regime of intermediate dispersion. This is in analogy to the dispersion ratios of several other III–V compounds (GaAs, GaSb, InN, InP, and InSb) and of most II–VI compounds (ZnS, ZnSe, ZnTe, CdS, and CdSe). The relatively low values of the dispersion ratios in all these materials are the reason why Varshni's formula (eq. (4)) has little chance to give adequate fits and parameter values for these materials (cf. Sections 4 and 5).

A relatively detailed information on the shape of the $E(T)$ dependence in ***gallium phosphide*** (GaP) *below* room temperature is provided e.g. by the absorption line position data, $E_{\mathrm{gbx}}(T)$, given by Dean et al. [21] for excitions weakly bound at iso-electronic nitrogen donors (see Fig. 7). In view of a much higher Debye temperature (of order 500 K), however, it appears useful for an appropriate estimation of the limiting slope to consider also the $E_{\mathrm{g}}(T)$ data set given by Lorenz et al. [22] (cf. Fig. 7). The $T \to 0$ limiting positions following from a simultaneous fitting of both data sets by eq. (1) are $E_{\mathrm{gbx}}(0) = 2.317$ eV and $E_{\mathrm{g}}(0) = 3.339$ eV. The latter differs by only 1 meV from the

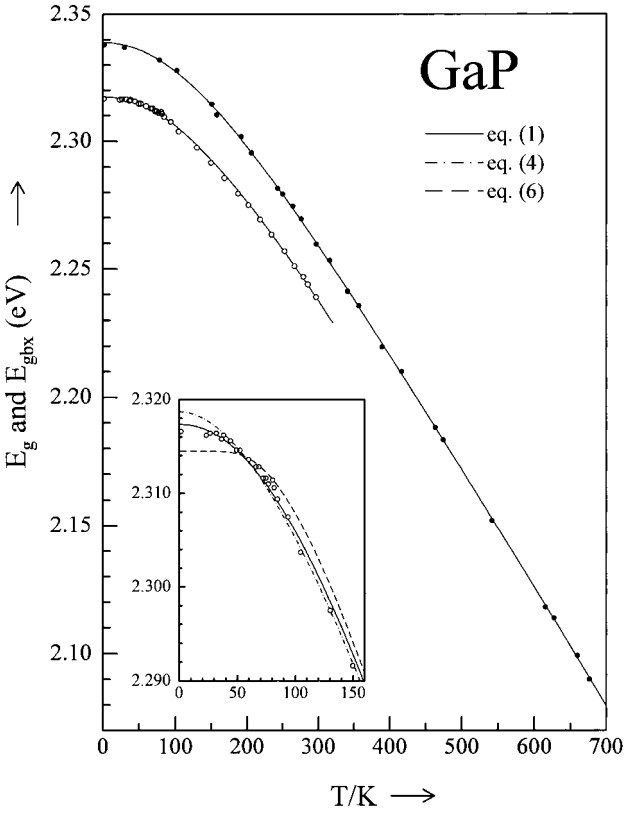


Fig. 7. Simultaneous fittings of the absorption line position data (empty circles) given by Dean et al. [21] for excitons weakly bound at iso-electronic nitrogen donors in gallium phosphide in combination with fundamental bandgap energy data (filled circles) given by Lorenz et al. [22]

repeatedly quoted $E_g(0)$ value of 3.338 eV [3, 22, 24], but it is by 11 meV lower than the value of $E_g(0) = 3.350$ eV given in [1]. In order to resolve this discrepancy, some more detailed $E_g(T)$ data (especially for the cryogenic region) would be necessary. Comparing the magnitude of $p = 2.09$ for GaP with $p$ values for other materials (in Table 1) we see that GaP represents one of the *few* cases where $p$ approaches relatively closely to the critical magnitude of two (where a qualitative change of the behavior of the slope, $S(T)$ (eq. (2)), between the regimes of intermediate and large dispersion takes place; cf. Section 4). This close approach to the regime of large dispersion is the cause of a somewhat closer approach between the curves following from eq. (1) and Varshni's formula (4) than in other materials (cf. the inset to Fig. 7; note that the variances due to the alternative fittings of the whole set of $E_{gbx}(T)$ and $E_g(T)$ data points are about 0.6 meV$^2$ for eq. (1), 1.1 meV$^2$ for eq. (4), and 2.2 meV$^2$ for eq. (6)).

For the case of ***gallium arsenide*** (GaAs) a high-precision $E_g(T)$ data set (see Fig. 8) was given by Grilli et al. [23] (a detailed numerical analysis of which has already been performed in [8]). However, the experimentally chosen break-off temperature (of 280 K in [23]) is significantly lower than the effective Debye temperature (of about 360 K [1]). Thus it appeared adequate to consider still some additional experimental $E_g(T)$ values as given e. g. by Panish and Casey [24], for 473 and 673 K (represented by filled circles in Fig. 8). Comparing the resulting parameter set (in Table 1) with the earlier one [8] (which resulted from a fit of merely the $E_g(T \leq 280$ K) data set [23] by eq. (1))

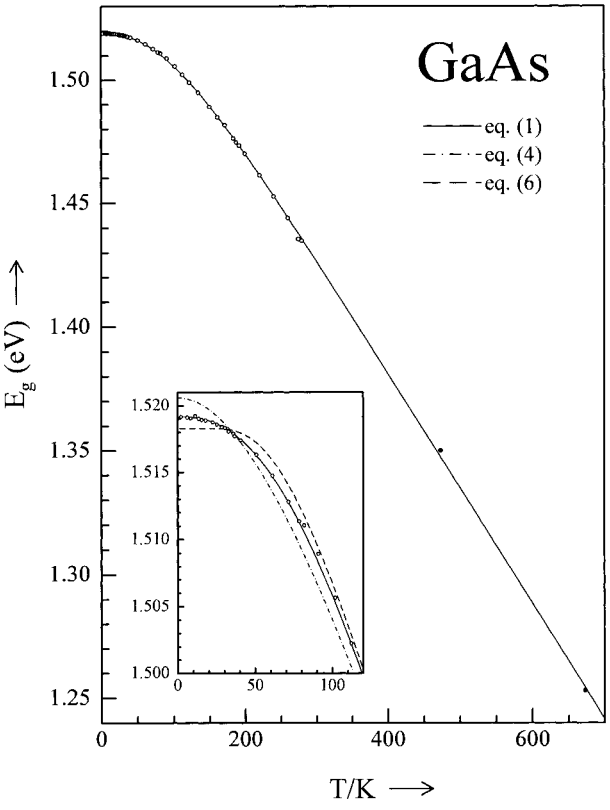


Fig. 8. Fittings of the high-precision bandgap energy data (empty circles) given for gallium arsenide by Grilli et al. [23] in combination with two further bandgap energy values given by Panish and Casey [24] (filled circles)

we see that the shifts involved by the inclusion of the two additional points [24] into the fitting process amount to only about 0.4% for $\alpha$, 1.5% for $\Theta_p$, and 3% for $p$. This indicates a high degree of stability (i.e. independence of the arbitrarily chosen break-off temperature for fittings and/or measurements) of the empirical parameter set due to eq. (1). In contrast to this, in the case of Varshni's formula (eq. (4)), the inclusion of these two additional experimental points into the least-mean-square fitting process (performed in analogy to most experimental papers with the *same* weight for all data points) leads to a jump of the $\alpha_{\mathrm{Var.}}$ value from 0.782 meV/K [8] to 0.528 meV/K (reduction by more than 30%) in combination with a jump of the $\beta$ value from 430 K [8] to 218 K (reduction by as much as 50%).

For the case of ***gallium antimonide*** (GaSb) we have analyzed the $E_g(T \leq 300\ \mathrm{K})$ data set given by Ghezzi et al. [25] (see Fig. 9). In view of the relatively low Debye temperature (of about 266 K), this data set should be largely sufficient for a proper estimation of the limiting slope. On the other hand, this data set is relatively scarce in the cryogenic region (cf. the inset to Fig. 9), so that in particular the present $p$ value cannot yet be considered as a definitive one.

The only $E_g(T)$ data set which we could find in literature for ***indium nitride*** (InN) was that given by Guo and Yoshida [26] (see Fig. 10). This data set is relatively scarce (consisting of only eleven data points). In addition to this, the experimental uncertain-

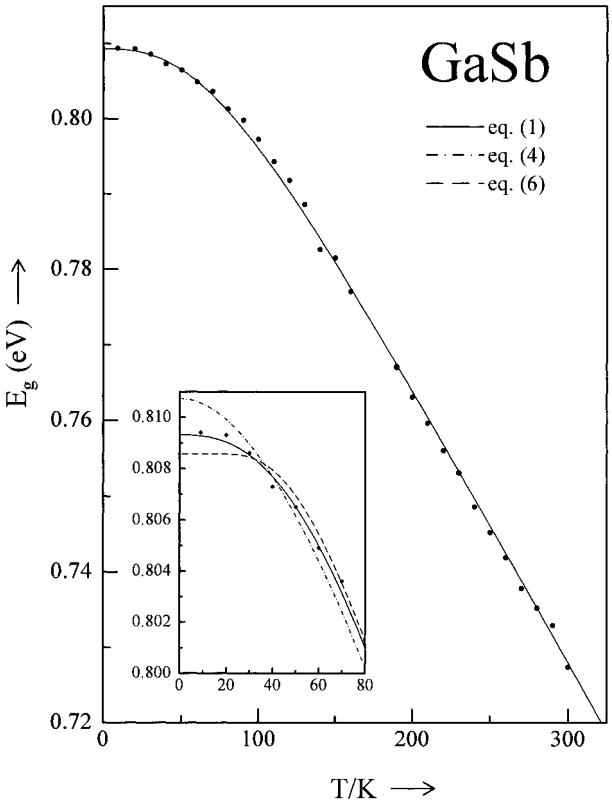


Fig. 9. Fittings of the bandgap energy data given for gallium antimonide by Ghezzi et al. [25]

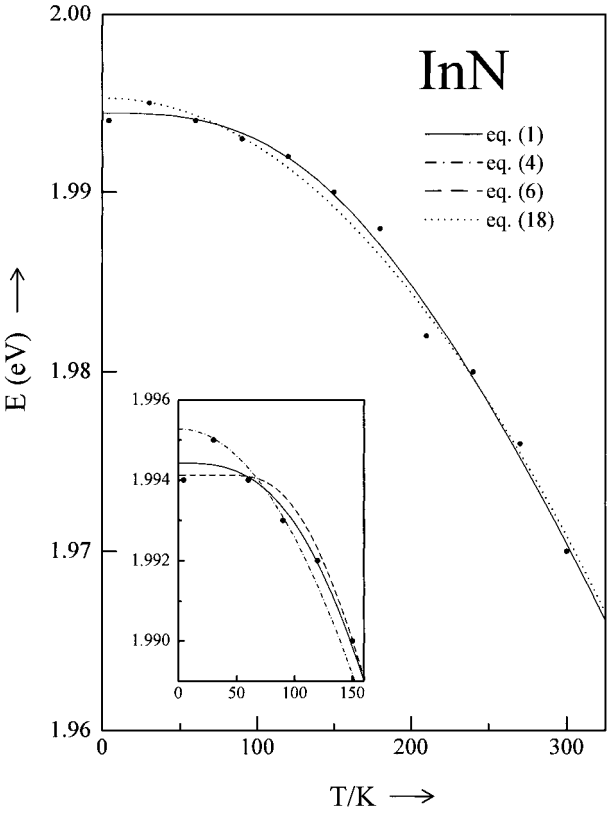


Fig. 10. Fittings of the bandgap energy data given for indium nitride by Guo and Yoshida [26]

ties (especially in the cryogenic region) are relatively large. The Debye temperature does not seem to be known for InN. From a comparison of the energies of optical phonons in all three group-III nitrides [1, 46], however, one can roughly estimate that $\Theta_D$ could be of order 700 K (±100 K). Thus the restricted $E_g(T \leq 300\ \mathrm{K})$ data set [26] (shown in Fig. 10) is clearly insufficient for a trustworthy estimation of empirical parameter sets. The $\alpha$ value of about 0.21 meV/K, which we have obtained by a fit using eq. (1), is *unusually low*. (Note that this is the lowest one for all materials listed in Table 1.) Of course, in view of the above arguments it is obvious that this value can be by no means considered as a definitive one. Possible future measurements, which might be performed beyond room temperature, cannot be excluded to lead to a largely different parameter constellation. Nevertheless, the present estimation of a preliminary $\alpha$ value for InN, which is by a factor of about three smaller than that for GaN (cf. Table 1), could be taken at least as an indication of a possibly *very strong composition dependence* of limiting slopes in ternary $In_xGa_{1-x}N$ compounds. Considering tentatively the estimated order of about 450 K for $\Theta_p$ in InN as adequate and assuming that the $\Theta_p/\Theta_D$ ratio for this material falls into the usual interval of 0.5 to 0.7 (in analogy to the majority of materials listed in Table 1), we come to an order-of-magnitude estimation for the Debye temperature in InN of $\Theta_D \approx$(650 to 900) K. This is consistent with the estimation quoted above.

For ***indium phosphide*** (InP) a rather dense set of exciton luminescence energy positions, $E_{gx}(T \lesssim 230\ \mathrm{K})$, has been given by Pavesi et al. [27] (see Fig. 11). In view of the fact that the Debye temperature (of about 420 K) is significantly higher than the break-off temperature [27], we have included (in analogy to GaP) a series of $E_g(T)$ data points due to Hang et al. [28] in combination with the rather accurately known $T \to 0$ bandgap energy value of $E_g(0) = 1.4239$ eV [27]. The associated $T \to 0$ limit for the exciton luminescence peak position is $E_{gx}(0) = 1.4181$ eV. The difference of $E_g(0) - E_{gx}(0) = 5.8$ meV is in reasonable agreement with the known exciton binding energy of $E_{bx} = 5.3$ meV [27].

For ***indium arsenide*** (InAs) a certain set of $E_g(T \leq 300\ \mathrm{K})$ data is available from a paper by Fang et al. [29]. In this case the break-off temperature is higher than the Debye temperature (cf. Table 1), so that such a data set can be globally expected to be sufficient for a reasonable parameter determination. On the other hand, this data set is very scarce (consisting of twelve data points in toto and containing only four data points in the $T < 100$ K region; see Fig. 6 in [29]). This does not seem to be sufficient for a trustworthy estimation of the dispersion ratio (3) (owing to an uncertainty for $p$ of an order $\pm 0.2$, in this case).

For ***indium antimonide*** (InSb) a certain set of $E_g(T \leq 300\ \mathrm{K})$ data is available again from the paper by Fang et al. [29] (which is reproduced here by the empty circles in

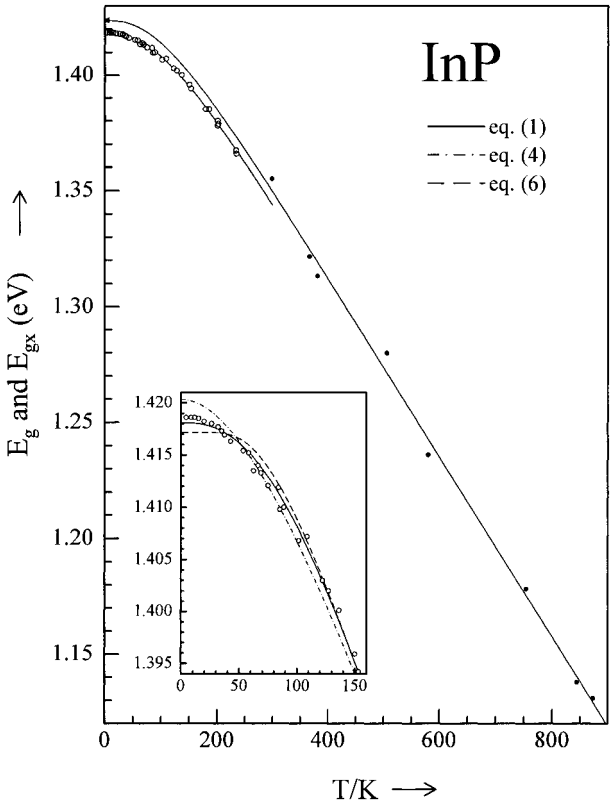


Fig. 11. Simultaneous fittings of the exciton luminescence energy data (empty circles) given for indium phosphide by Pavesi et al. [27] in combination with bandgap energy data (filled circles) given by Hang et al. [28]. The filled triangle represents the $T \to 0$ bandgap energy value of $E_g(0) = 1.4239$ eV [27]

Fig. 12). The break-off temperature is in this case even by a factor of 1.5 *higher* than the Debye temperature (Table 1). Thus, at first sight, no additional $E_g(T > 300\ \mathrm{K})$ data would seem to be necessary for a reasonable fixation of the parameter set. Unfortunately, the available $E_g(T \leq 300\ \mathrm{K})$ data set is again very scarce (consisting of 11 data points in toto and containing only five data points in the $T < 100$ K region; see Fig. 6 in [29]). In view of this scarcity we have made use of the possibility (in analogy to Ref. [49]) to get some additional information by including a certain $E_g(T \geq 300\ \mathrm{K})$ data set given by Liu and Maan [30]. Unfortunately, the error bars for the latter data set were found to be by a factor of about three to four larger than in the case of the $E_g(T \leq 300\ \mathrm{K})$ set due to Fang et al. [29]. In such a case it would not be adequate to perform the fitting process (as usual) with the same weight for all data points. Instead, according to [50], one has to endow the data points in question with weighting factors which are inversely proportional to the square of the corresponding error bars (cf. [23] and [32]). This means, for the data constellation in consideration, a reduction of the weight for the $E_g(T \geq 300\ \mathrm{K})$ data points [30] by a factor of order ten in comparison with that for the $E_g(T \leq 300\ \mathrm{K})$ data points [29]. Within this choice of weighting factors we have obtained the parameter values listed for InSb in Table 1. Their comparison with those obtained for InAs shows above all a relatively large difference between $p$ values (and thus of the corresponding dispersion ratios) for both materials. In view of

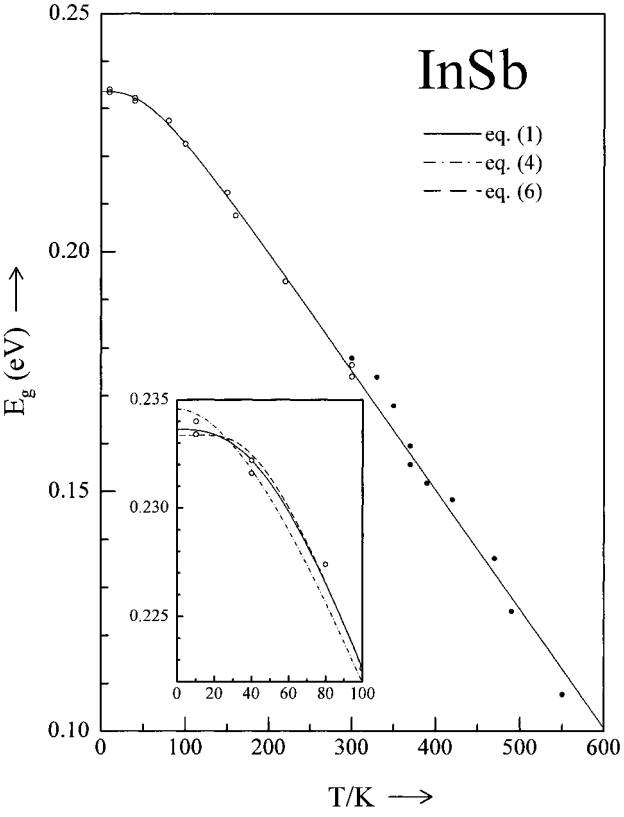


Fig. 12. Fittings of the bandgap energy data given for indium antimonide by Fang et al. [29] (empty circles) in combination with further bandgap energy data given by Liu and Maan [30] (filled circles)

the scarcity of the $E_g(T \leq 300\ \mathrm{K})$ data sets [29] available hitherto, the actual degree of adequacy of these two different $p$ values cannot be assessed. A trustworthy estimation of dispersion ratios for these two materials could only be given in disposing of much *denser* $E_g(T)$ data sets.

### *3.3 Analyses and results for II–VI compounds*

In analogy to most gallium- and indium-based III–V compounds, a considerable variety of $E_g(T)$ and $E_{gx}(T)$ data sets has been published during the past three decades also for II–VI compounds (for a list of references see [31, 32]). The majority of these data sets, however, can be readily seen to be rather scarce, rather restricted (usually to $T \leq 300$ K) and/or relatively inaccurate, so that they appear more or less insufficient for a trustworthy determination of empirical parameter sets (independently of the analytical model used). In order to obtain more informative experimental data fields, which should be suitable in particular for incisive numerical tests of qualitatively different analytical models, a larger group of researchers has performed recently a series of comprehensive experimental studies for zinc chalcogenides (see [31]). Special experimental efforts were necessary for the wide bandgap materials ***zinc sulphide*** (ZnS) and ***zinc selenide*** (ZnSe), since the corresponding Debye temperatures are relatively high ($\Theta_D \approx 440$ K and 340 K, respectively). Two qualitatively different methods have been combined in [31] in order to determine the 1s exciton peak energy positions from cryogenic temperatures up to about $4\Theta_D/3$ [31], namely: absorption measurements performed within the ranges (2 to 387) K for ZnS [31] or (4 to 280) K for ZnSe [32] and reflectance measurements performed within the ranges (303 to 541) K for ZnS or (300 to 500) K for ZnSe. In contrast to both wide bandgap materials, the Debye temperature in the case of ***zinc telluride*** (ZnTe) is relatively low ($\Theta_D \approx 260$ K). Absorption measurements within the range (2 to 291) K appeared thus sufficient for a proper parameter determination in this material (for all further details see [31]). Here we show only (in Fig. 13) the characteristic combination of $E_{1s}(T)$ data points obtained by the two different methods for the case of ZnSe. The total data set consists of a series of *absorption* data points (the relatively high density of which in the cryogenic region enables a trustworthy determination of the dispersion-related parameter $p$ in eq. (1)) and a series of reflectance data points covering the range between 300 and 500 K. Let us compare the present parameter values obtained by fitting the *whole* data set for ZnSe with eq. (1) (given in Table 1) with the earlier values given in [32] (which resulted from a fit of merely the $E_{1s}(T \leq 280\ \mathrm{K})$ data set [32] by the same equation). From this comparison we see that the parameter shifts caused by the inclusion of the 21 additional points [31] (filled circles in Fig. 13) into the fitting process amount to only about 1.2% for $\alpha$, 1.6% for $\Theta_p$, and 0.4% for $p$. The small sizes of these shifts show that the empirical parameter sets resulting from fittings by eq. (1) are practically *independent* of the break-off temperature (chosen for fittings or in measurements). In contrast to this, Varshni's parameter set shows a high degree of instability. The inclusion of the 21 additional experimental points into the fitting process (performed as usual with the *same* weight for all data points) leads to a jump of the $\alpha_{Var.}$ value from 0.765 to 0.558 meV/K (reduction by 27%) in combination with a jump of the $\beta$ value from 338 K [8] to 187 K (reduction by 45%). These characteristic jumps of Varshni parameter values for ZnSe, which are caused simply by a change of the (accidentally) chosen

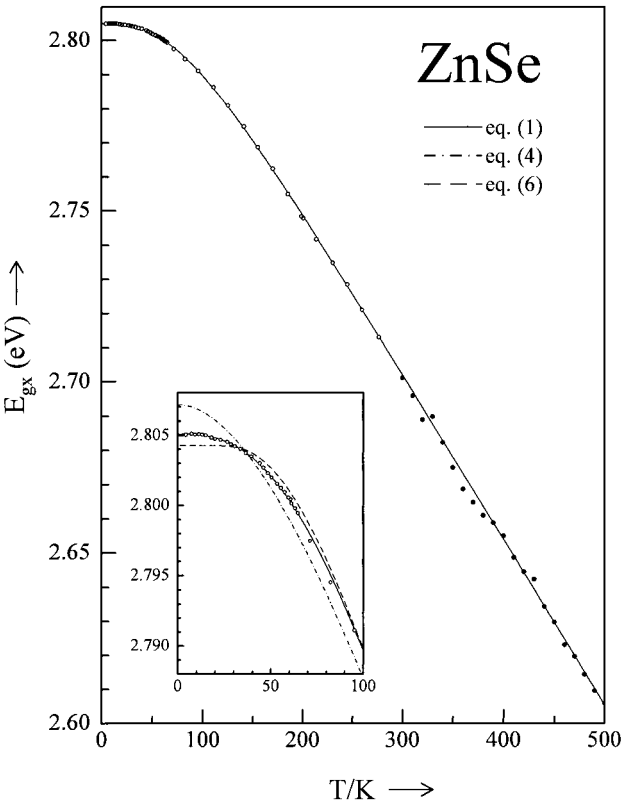


Fig. 13. Fittings of the exciton peak energy positions obtained for zinc selenide by Pässler et al. [31] (empty and filled circles are representing the results due to absorption and reflectance measurements, respectively)

break-off temperature for the set of data points included into the fitting process, are of the same order of magnitude as in the case of GaAs (cf. Sections 3.2 and 5.1).

Several useful $E_g(T)$ data sets are available for ***cadmium sulphide*** (CdS) [33 to 36]. Their fittings by the analytical models in consideration (i.e. eqs. (1), (4), and (6)) have already been performed and the results have been discussed in detail in Ref. [9]. Thus we quote here only (in Table 1) the parameter values due to the fit by eq. (1).

A useful $E_{gx}(T)$ data set has been given by Logothetidis et al. [37] for the temperature dependence of the A exciton excitation energies in hexagonal ***cadmium selenide*** (CdSe). The fitting by eq. (1) gives a $T \to 0$ position of $E_{gx}(0) = 1.831$ eV. Combining the latter with an exciton binding energy of $E_{bx} = 0.015$ eV [1] we obtain a $T \to 0$ energy for the A gap of $E_g(0) = 1.846$ eV.

Comparing the $\Theta_p/\Theta_D$ and $\Delta\varepsilon/\bar{\varepsilon}$ ratios (in Table 1) obtained for hexagonal CdS and CdSe with those for cubic ZnS, ZnSe, and ZnTe we find that these values are ranging throughout within rather small intervals ($\Theta_p/\Theta_D \approx 0.53$ to 0.56 and $\Delta\varepsilon/\bar{\varepsilon} \approx 0.39$ to 0.44). In contrast to the latter, for the case of cubic ***cadmium telluride*** (CdTe), we have obtained from a fit of the $E_g(T \leq 300$ K) data set given by Laurenti et al. [38] by eq. (1) considerably higher values for both ratios. However, it cannot be excluded that this difference is a numerical artifact. (Note that, due to the extremely small size of Fig. 3 in Ref. [38], the redigitalization of these $E_g(T)$ data especially in the cryogenic region, $T < 50$ K, could be connected with considerable uncertainties.) In addition to this, a

comparison of the $E_g(T)$ data set given in [38] with data sets given by other authors (see e.g. [51 to 53]) reveals rather large differences. Values for the high-temperature slope, $\alpha$, as following from fittings vary between 0.3 meV/K [38] and 0.45 meV/K [53]. This large scattering of estimated $\alpha$ values is closely connected with a large uncertainty range for the *room* temperature bandgap energy. The reported values are ranging between 1.529 eV [38] and about 1.48 eV [53] (corresponding to an unusually high uncertainty of about 50 meV). On the other hand, it follows even from these largely different data sets [51 to 53], for CdTe, that the parameter $p$ in eq. (2) should actually be *smaller* than two, i.e. the assignment to the regime of *large* dispersion, $\Delta\varepsilon/\bar{\varepsilon} > 3^{-1/2} = 0.577$, seems to be adequate. Such a large dispersion in combination with a rather low value for the effective phonon temperature, $\Theta \approx 100$ K, are the reasons why, in this particular case, even Varshni's formula (4) is capable of giving nearly the same values for $\alpha$ as eqs. (1) and (6). The fits by eqs. (1) and (4) are practically indistinguishable (in analogy to the case of AlSb).

## 4. Analytical Distinctions

From the insets to Figs. 2 to 13 we see that, especially in the cryogenic region, one is usually concerned with an obviously typical constellation of alternative model curves, namely: the temperature dependencies imputed by the three-parameter formulae (4) and (6) are too strong or too weak, respectively. In contrast to the latter, the four-parameter curves due to eq. (1) show a behavior which is somehow *intermediate* between both extremes (4) and (6) and give throughout the *best* fits of the measured $E(T)$ dependencies (as shown by absolute minimum values for residual variances).

### *4.1 Qualitative difference between four- and three-parameter models*

For a proper understanding of this typical state of affairs it is useful to exhibit clearly the structural deficiencies of eqs. (6) and (4), which are responsible for their usual incapability of giving fits with variances as low as those due to eq. (1). Such an analytical study seems to be especially important with respect to Varshni's formula, eq. (4) (in view of its frequent use in experimental literature during the past 30 years). For that purpose we introduce (in analogy to [8]) a dimensionless energy variable, $\eta$, by referring the magnitude of the gap energy change, $E(0) - E(T)$, to the material-specific energy unit $\alpha\Theta_p/2$, i.e. $\eta \equiv 2(E(0) - E(T))/\alpha\Theta_p$. Analogously we introduce a dimensionless temperature variable, $\xi$, by referring $T$ to the material-specific temperature unit $\Theta_p/2$, i.e. $\xi \equiv 2T/\Theta_p$. In terms of these novel variables we can rewrite eq. (1) in the equivalent form

$$\frac{2(E(0) - E(T))}{\alpha\Theta_p} = \eta_p\left(\frac{2T}{\Theta_p}\right), \quad \text{where} \quad \eta_p(\xi) \equiv \sqrt[p]{1 + \xi^p} - 1\,. \tag{7}$$

From (7) we see that the very *shape* of the functional dependence of the relative energy drop, $\eta_p(\xi)$, on $\xi$ is determined *exclusively* by the parameter $p$ (i.e. by the dispersion ratio (3)). In contrast to this, the parameters $\alpha$ and $\Theta_p$ are controlling only the *scales* of the variables $\eta$ and $\xi$ with respect to the original $E$ and $T$ axes. This means that $E(T)$ dependencies characterized by the *same* $p$ in (7), but different parameters $\alpha$ and $\Theta_p$, can be brought to perfect *coincidence* by performing nothing but convenient

*contractions* or *dilatations* of one of these curves in vertical and horizontal directions (in combination, of course, with an appropriate shift of the $E(0)$ position in vertical direction). In contrast to this, curves with *different p* can *never* be brought to coincidence, which contractions or dilatations in both orthogonal directions (by changing $\alpha$ and $\Theta_p$) would ever be performed.

On the basis of this consideration one can see readily why it is usually impossible to achieve an adequate fit of a given $E(T)$ curve by means of eq. (4) or (6). In analogy to (7) we can represent Varshni's eq. (4) in the equivalent form

$$\frac{E(0) - E_{\text{Var.}}(T)}{\alpha_{\text{Var.}}\beta} = \eta_{\text{Var.}}\left(\frac{T}{\beta}\right), \quad \text{where} \quad \eta_{\text{Var.}}(\xi) \equiv \frac{\xi^2}{1+\xi} \tag{8}$$

represents an a priori *fixed* dependence on $\xi \equiv T/\beta$. Analogously we can rewrite the model function (6) of Bose-Einstein type in the equivalent form

$$\frac{2(E(0) - E_{\text{B.-E.}}(T))}{\alpha\Theta} = \eta_{\text{B.-E.}}\left(\frac{2T}{\Theta}\right), \quad \text{where} \quad \eta_{\text{B.-E.}}(\xi) \equiv \coth\left(\frac{1}{\xi}\right) - 1 \tag{9}$$

is an a priori *fixed* dependence on $\xi \equiv 2T/\Theta$. From (8) and (9) we see now clearly that, by changing the magnitudes of the parameters $E(0)$, $\alpha_{\text{Var.}}$, and $\beta$ in (8) or $E(0)$, $\alpha$, and $\Theta$ in (9), we can only realize shifts along the energy axis in combination with contractions or dilatations of the given curve in both orthogonal directions. Such changes of $E_{\text{Var.}}(T)$ or $E_{\text{B.-E.}}(T)$ curves due to parameter changes during a least-mean-square procedure are thus corresponding only to changes of *projections* of firmly chosen $\eta_{\text{Var.}}(\xi)$ (8) or $\eta_{\text{B.-E.}}(\xi)$ (9) curves out of the $\eta$-$\xi$-plane into the $E$-$T$-plane. At the same time, the model-specific shapes ("fingerprints") of both curves, $\eta_{\text{Var.}}(\xi)$ (8) or $\eta_{\text{B.-E.}}(\xi)$ (9), remain *fixed*. This means that one has no chance to produce an actual *fit* (in the proper sense of this word) when the characteristic shape, $\eta(\xi)$, of a measured $E(T)$ curve is not accidentally the same as either $\eta_{\text{Var.}}(\xi)$ or $\eta_{\text{B.-E.}}(\xi)$. The numerical studies of the present paper have shown that such a coincidence is a rarity. (Note that we have found an approximate equality, $\eta(\xi) \approx \eta_{\text{Var.}}(\xi)$, just for the cases AlSb and CdTe, whereas $\eta(\xi)$ is clearly different from $\eta_{\text{Var.}}(\xi)$ for all other materials.) Usually the characteristic shape, $\eta(\xi)$, of a given data set is found to be somehow *intermediate* between these fixed extrema, $\eta_{\text{Var.}}(\xi)$ and $\eta_{\text{B.-E.}}(\xi)$, and can be represented in good approximation by the flexible shape function $\eta_p(\xi)$ [8] (eq. (7)). This is clearly shown by the insets to Figs. 2 to 13.

At the same time we see also from these insets that the systematic deviations of the $E_{\text{Var.}}(T)$ or $E_{\text{B.-E.}}(T)$ curves from measured $E(T)$ dependencies use to amount "only" to some *few* meV. Within the frame of various practical application, deviations of this order may sometimes be negligible. This could lead to the suggestion that even a relatively simple analytical model like eq. (4) or (6) might be of practical use. This applies at least to the model of Bose-Einstein type (eq. (6)). Indeed, apart from the notorious misfits (due to its plateau behavior) in the *cryogenic* region, this model uses to give reasonable results. Many numerical studies have shown that the fitted parameter values, $\alpha$ and $\Theta$, are as a rule physically adequate. This is highly important for extrapolations of fitted curves beyond the experimentally chosen break-off temperature (cf. the inset to Fig. 1). In contrast to the latter model, Varshni's formula gives in many cases largely inadequate (usually too high) values for the limiting slope, so that this model is not

suitable for extrapolations beyond the break-off temperature. Furthermore it is obvious that Varshni's temperature parameter $\beta$ is an arbitrarily chosen one. Its value gives as a rule no information on a basic physical feature of the system (like the effective phonon temperature or the Debye temperature).

### *4.2 Distinction between alternative slope functions*

We can get more insight into the qualitative differences between the analytical models in discussion by considering the different behaviors of the slopes, $S(T) = -\mathrm{d}E(T)/\mathrm{d}T$ (= entropies [3, 7], eq. (2)). From eq. (1) follows readily the slope (2) to be given by [7]

$$S(T) = \alpha\left(1 + \left(\frac{\Theta_p}{2T}\right)^p\right)^{1/p-1} = \alpha\,\sigma_p\left(\frac{2T}{\Theta_p}\right),$$

where

$$\sigma_p(\xi) = \eta_p'(\xi) = (1 + \xi^{-p})^{1/p-1} \tag{10}$$

is the first derivative of $\eta_p(\xi)$ (eq. (7)). Typical shapes of this $\sigma_p(\xi)$ function (10) are shown for $p$ = 2.0, 2.5, and 3.0 in Fig. 14. A characteristic feature of the $\sigma_{p>2}(\xi)$ curves, which is of great importance for adequate fittings, is the occurrence of an *S-curve-like* behavior. In order to get more information on the interval of dispersion ratios where we are concerned with this feature it is necessary to investigate higher order derivatives. The second derivative of the slope, $S(T)$ (10), reads

$$\frac{\mathrm{d}^2S(T)}{\mathrm{d}T^2} = \alpha\left(\frac{2}{\Theta_p}\right)^2 \sigma_p''\left(\frac{2T}{\Theta_p}\right), \quad \text{where} \quad \sigma_p''(\xi) = \frac{(p-1)\,\xi^{p-3}}{(1+\xi^p)^{3-1/p}}\left((p-2) - (p+1)\,\xi^p\right). \tag{11}$$

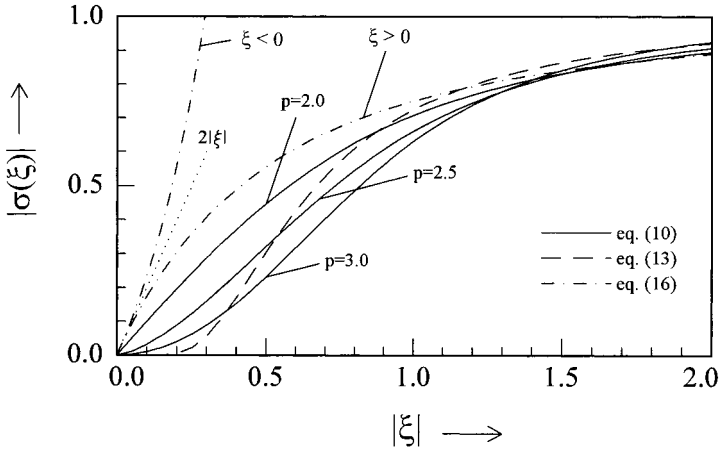


Fig. 14. Comparison of the characteristic shapes of the *adjustable* ($p$-dependent) slope function $\sigma_p(\xi)$ (10) (due to the *four*-parameter model used in the present paper, eq. (1)) in comparison with the *inflexible* counterparts $\sigma_{\mathrm{B.-E.}}(\xi)$ (13) (due to the Bose-Einstein-related model, eq. (6)) and $\sigma_{\mathrm{Var.}}(\xi)$ (16) (due to Varshni's formula, eq. (4))

The latter vanishes at $\xi_p = \sqrt[p]{(p-2)/(p+1)}$, i. e. the slope function, $S(T)$ (10), has for $p > 2$ a *point of inflection* which is located at

$$T_p \equiv \frac{\Theta_p}{2}\xi_p = \frac{\Theta_p}{2}\sqrt[p]{\frac{p-2}{p+1}} \tag{12}$$

(in accordance with the above definition of $\xi$, i.e. $\xi \equiv 2T/\Theta_p$). We are thus concerned, for any $p > 2$, with a more or less pronounced S-curve-like behavior of the slope (entropy). This concerns (in accordance with (3)) the experimentally dominating region of *intermediate* to *small* dispersion. On the other hand, such a behavior is absent for $p < 2$ (where $T_p$ (12) ceases to be real). The particular parameter value $p = 2$ turns thus out to represent a critical point where we are concerned with a qualitative change of the behavior of the slope function $S(T)$ (10). According to eq. (3), the particular parameter value of $p = 2$ corresponds to a dispersion ratio of $\Delta\varepsilon/\bar{\varepsilon} = 3^{-1/2} = 0.577$. This connection suggests to look upon just the latter value as the characteristic boundary between the regimes of intermediate and large dispersion (cf. Section 1).

A similar property as the $S(T)$ function (eq. (10)), for $p > 2$, has also the counterpart due to the Bose-Einstein-related model. The corresponding slope follows from (6) to be given by

$$S_{\mathrm{B.-E.}}(T) = \alpha\left(\frac{\frac{\Theta}{2T}}{\sinh\frac{\Theta}{2T}}\right)^2 = \alpha\sigma_{\mathrm{B.-E.}}\left(\frac{2T}{\Theta}\right),$$

where

$$\sigma_{\mathrm{B.-E.}}(\xi) \equiv \eta'_{\mathrm{B.-E.}}(\xi) = \left(\xi\sinh\left(\frac{1}{\xi}\right)\right)^{-2} \tag{13}$$

is the first derivative of $\eta_{\mathrm{B.-E.}}(\xi)$ (9). This characteristic slope function, $\sigma_{\mathrm{B.-E.}}(\xi)$, is seen from Fig. 14 to have a very strongly pronounced S-curve-like behavior. Within this model the second derivative of the slope, $S_{\mathrm{B.-E.}}(T)$ (14), reads

$$\frac{\mathrm{d}^2 S_{\mathrm{B.-E.}}(T)}{\mathrm{d}T^2} = \alpha\left(\frac{2}{\Theta}\right)^2 \sigma''_{\mathrm{B.-E.}}\left(\frac{2T}{\Theta}\right),$$

where

$$\sigma''_{\mathrm{B.-E.}}(\xi) = \frac{2(3(\xi - \coth(\xi^{-1}))^2 - 1)}{\xi^6(\sinh(\xi^{-1}))^2}. \tag{14}$$

The latter vanishes at $\xi_{\mathrm{B.-E.}} = 0.445319$, i.e. the model-specific slope function $S_{\mathrm{B.-E.}}(T)$ (13) has *always* a *point of inflection*, which is located at

$$T_{\mathrm{B.-E.}} \equiv \frac{\Theta}{2}\,\xi_{\mathrm{B.-E.}} = 0.445319\,\frac{\Theta}{2} \tag{15}$$

(in accordance with the above definition of $\xi$, i.e. $\xi \equiv 2T/\Theta$). Fig. 14 shows that, due to the plateau behavior of $\sigma_{\mathrm{B.-E.}}(\xi)$, at $\xi < 0.2$, the S-curve-like shape of the latter is much more pronounced than that of the $\sigma_p(\xi)$ function (10), for $2 < p \leq 3$.

Consider finally Varshni's formula, whose entropy function is known to be given by [3, 7]

$$S_{\mathrm{Var.}}(T) = \alpha_{\mathrm{Var.}} \frac{T(2\beta + T)}{(\beta + T)^2} = \alpha_{\mathrm{Var.}}\, \sigma_{\mathrm{Var.}}\left(\frac{T}{\beta}\right),$$

where

$$\sigma_{\mathrm{Var.}}(\xi) \equiv \eta'_{\mathrm{Var.}}(\xi) = \frac{\xi(2+\xi)}{(1+\xi)^2}\,. \tag{16}$$

The plot of this $\sigma_{\mathrm{Var.}}(\xi)$ function in Fig. 14 shows that the latter has *no inflection point* at all, neither for $\xi \equiv T/\beta > 0$ (corresponding to a *positive* $\beta$ value) nor for $\xi \equiv T/\beta < 0$ (corresponding to a *negative* $\beta$ value). Calculating from (16) the second derivative of Varshni's slope function we obtain

$$\frac{\mathrm{d}^2 S_{\mathrm{Var.}}(T)}{\mathrm{d}T^2} = \frac{-6\alpha_{\mathrm{Var.}}\beta^2}{(\beta + T)^4} = \frac{\alpha_{\mathrm{Var.}}}{\beta^2}\ \sigma''_{\mathrm{Var.}}\left(\frac{T}{\beta}\right),$$

where

$$\sigma''_{\mathrm{Var.}}(\xi) = \frac{-6}{(1+\xi)^4} < 0\,, \tag{17}$$

for any $\xi \geq 0$ and $\xi \leq 0$. (Note that $\sigma''_{\mathrm{Var.}}(\xi)$ tends to $-\infty$ at the singular point $\xi \to -1$.) This complete absence of a point of inflection in Varshni's slope function, $S_{\mathrm{Var.}}(T)$ [3, 7] (eq. (16)), has heavy consequences for parameter sets.

## 5. Parameter Set Inconsistencies Due to Varshni's Model

### *5.1 Overestimation of limiting slopes and jumps of parameter sets*

Using the parameter values $\alpha$, $\Theta_p$ and $p$ given for Si and Ge in Table 1 we have calculated by means of eq. (10) the corresponding slopes, $S(T)$. These are plotted together with their counterparts in consideration, i.e. $S_{\mathrm{B.-E.}}(T)$ (13) and $S_{\mathrm{Var.}}(T)$ (16), in Fig. 15. The comparison of the high-temperature parts (extrapolations up to 1000 K) of these three curves shows that the limiting slopes for the $S_{\mathrm{Var.}}(T)$ curves [3] are *significantly higher* than those due to $S(T)$ (10) and $S_{\mathrm{B.-E.}}(T)$ (13). These pronounced differences between magnitudes estimated for limiting slopes are a general consequence of the fact that Varshni's model has no possibility to adjust its slope to the S-curve-like shape, which is characteristic for the region of intermediate to small dispersion. Yet, due to rather different positions of the points of inflection, $T_{\mathrm{infl}}$ (12), for both materials, the degrees of overestimation of the limiting slopes for both materials are largely different. The experimental break-off temperatures $T_{\mathrm{max}}$ are about 415 K (Table 1), for both materials. Due to a relative low position of the point of inflection in Ge, $T_{\mathrm{infl}} \approx 46$ K, the ratio $T_{\mathrm{max}}/T_{\mathrm{infl}} \approx 9$ is relatively large. Thus the convex part of the experimentally covered $S(T)$ curve is largely dominating. This requires, within the frame of Varshni's model, a relatively close approach of the $S_{\mathrm{Var.}}(T)$ curve in the upper part. This is reflected by a limiting slope parameter of $\alpha_{\mathrm{Var.}}$ = 0.477 meV/K [3], which is by "only" about 17% higher than the $\alpha$ values following from the fits by eqs. (1) (cf. Table 1) and (6). The situation is significantly different, however, in the case of silicon. Due to a

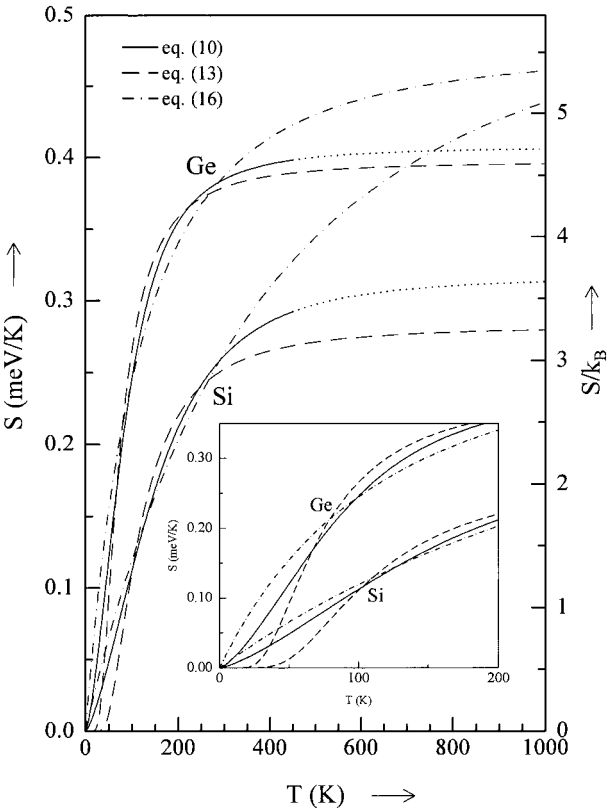


Fig. 15. Temperature dependencies of the slopes (2) as following from the alternative fittings of the temperature dependencies of the gaps in silicon [13, 14] (Fig. 3) and germanium [15] (Fig. 4). The inset shows in more detail the qualitative difference between the *S-curve-like* behavior of the slope functions (10) and (13) due to the four-parameter representation (1) and the Bose-Einstein-related model function (6), on the one hand, and the exclusively *convex* behavior of their counterpart (16) resulting from Varshnís formula (4)

relative high position of the point of inflection, $T_{\text{infl}} \approx 75$ K, the characteristic temperature ratio for Si is $T_{\max}/T_{\text{infl}} \approx 5.5$ (i.e. significantly lower than in Ge). This means that the convex part of the experimentally covered $S(T)$ curve in the case of Si is less dominating than in the case of Ge. The numerical consequence for Si (with respect to the experimental data set constellation shown in Fig. 3) is a limiting slope parameter of $\alpha_{\text{Var.}} = 0.537$ meV/K. The comparison with Table 1 shows that this values *overestimates* the limiting slope, $\alpha \equiv S(\infty)$, for Si by about 70%. On the basis of a large series of analogous numerical analyses we can say that, within the usual Varshni regime (i.e. for *positive* $\alpha_{\text{Var.}}$ and $\beta$ values), the $\alpha_{\text{Var.}}$ values obtained by numerical similations are throughout *larger* than the limiting slopes, $\alpha \equiv S(\infty)$, following from eqs. (1) and (6). In particular one can conclude from a variety of such numerical analyses that the relative size of overestimation, i.e. the ratio $(\alpha_{\text{Var.}} - \alpha)/\alpha > 0$, is closely related to the degree of dominance of the convex part of corresponding $S(T)$ function (10). In general one finds:

The *smaller* the characteristic temperature ratio, $T_{\max}/T_{\text{infl}}$, for a given data set is, the *larger* are the numerical values obtained for Varshni's parameters $\alpha_{\text{Var.}}$ and $\beta$.

This means that both parameters are primarily a function of the actual choice of the break-off temperature, $T_{\max}$, instead of giving objective quantitative information on basic physical properties of the material in question. These peculiar dependencies, $\alpha_{\text{Var.}}(T_{\max})$ and $\beta(T_{\max})$, involve in particular large *jumps* of both parameter values

when the break-off temperature, $T_{max}$, is changed significantly (due to different choices of $T_{max}$ by the individual researchers). We have already given above, for the cases of GaAs and ZnSe, typical examples of large parameter jumps due to changes of the break-off temperatures. Especially instructive for contemporary studies of nitrides could be the case of GaN [20]. We have plotted in Fig. 16 the $S(T)$ curve as following from eq. (10), with parameter values given for the hexagonal $GaN/Al_2O_3$ layer [20] in Table 1. The corresponding inflection temperature, $T_{infl}$, follows from (12) to be located at about 128 K. Despite of the relatively high position of the latter, the characteristic temperature ratio is still rather large, $T_{max}/T_{infl} \approx 8.3$ (due to the unusually high break-off temperature, $T_{max} \approx 1067$ K, chosen by Herr [20]). Consequently, the upper (convex) part of the $S(T)$ curve is largely dominating. A fit of the whole data set (Fig. 6) by Varshni's formula (4) gives a limiting slope parameter of $\alpha_{Var.} = 0.729$ meV/K in combination with $\beta = 579$ K (in accordance with [20]). The comparison with $\alpha$ in Table 1 shows that the overestimation of the limiting slope amounts in this case to "only" about 22%. Let us now break off Herr's data set [20] at 300 K (in analogy to the usual breaking-off of experimental measurements for GaN and related materials in most recent publications). The resulting parameter values are $\alpha_{Var.} = 3.05$ meV/K in combination with $\beta = 3893$ K. Thus the reduction of $T_{max}$ from 1067 to 300 K leads to jumps of Varshni's parameter values over almost an order of magnitude (by a factor of five for $\alpha_{Var.}$ and a factor 7.7 for $\beta$). This huge degree of arbitrariness of $\alpha_{Var.}$ and $\beta$ values, for

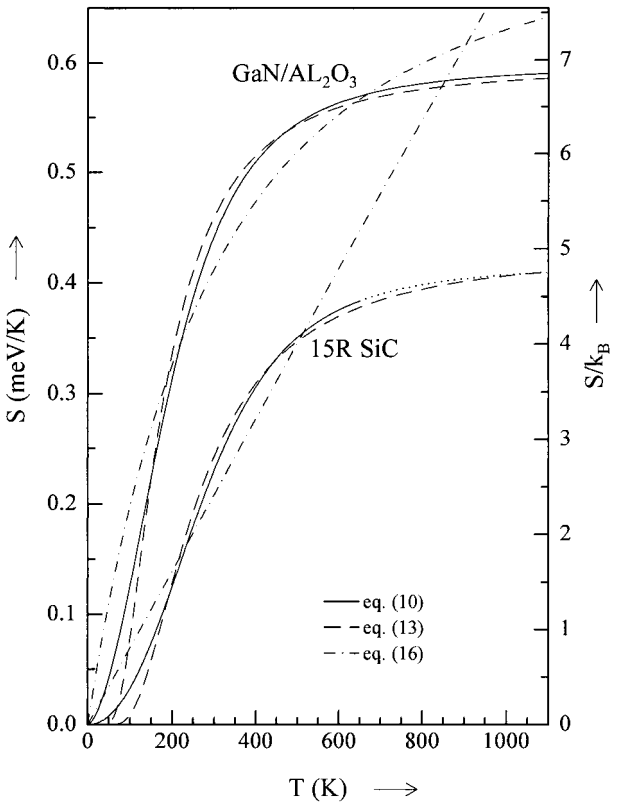


Fig. 16. Temperature dependencies of the slopes (2) associated with alternative fittings of the temperature dependencies of the gaps in 15R SiC [11] (Fig. 2) and hexagonal GaN [20] (Fig. 6). The approximate *straight* line behavior of the $S_{Var.}(T)$ function (eq. (16)) for the case of 15R SiC corresponds to the *floating* regime, $\alpha_{Var.} \to \infty$ and $\beta \to \infty$ (cf. Section 5.2)

a wide bandgap material like GaN, largely invalidates attempts to compare the results obtained by different authors via published $\alpha_{\text{Var.}}$ and $\beta$ values.

### *5.2 Floating of parameter sets*

We have plotted in Fig. 16 the $S(T)$ curve for 15R SiC as following from eq. (10), with parameter values given in Table 1. The corresponding inflection temperature follows from (12) to be unusually high in this case, $T_{\text{infl}} = 217$ K. Comparing the latter with the experimental break-off temperature, $T_{\text{max}} = 645$ K, we see that the characteristic temperature ratio is rather low, $T_{\text{max}}/T_{\text{infl}} \approx 3$. Consequently, in contrast to the examples given in Section 5.1, the usual dominance of the upper (convex) part is drastically reduced. Actually it appears from Fig. 16 that the lower (concave) part of the $S(T)$ curve is nearly so pronounced as its upper (convex) part. A quite analogous situation seems to be given also for the case of InN (see Fig. 17) due to a rather low break-off temperature ($T_{\text{max}} = 300$ K). Consequently, owing to the complete absence of an inflection behavior of the $S_{\text{Var.}}(T)$ function (eq. (16)), Varshni's model can cope with such a situation only by approximating the S-curve-like behavior of the slope by some *linear* dependence, $S_{\text{Var.}}(T) \propto T$. (Note that this limiting behavior of $S_{\text{Var.}}(T)$ (16) corresponds to the linear $\sigma_{\text{Var.}}(\xi) \rightarrow 2\xi$ asymptote of (16), for $|\xi| \ll 1$. This is represented by a dotted line in Fig. 14.) Yet, a *linear* $T$-dependence of the slope, $S(T) \propto T$ (for eq. (2)),

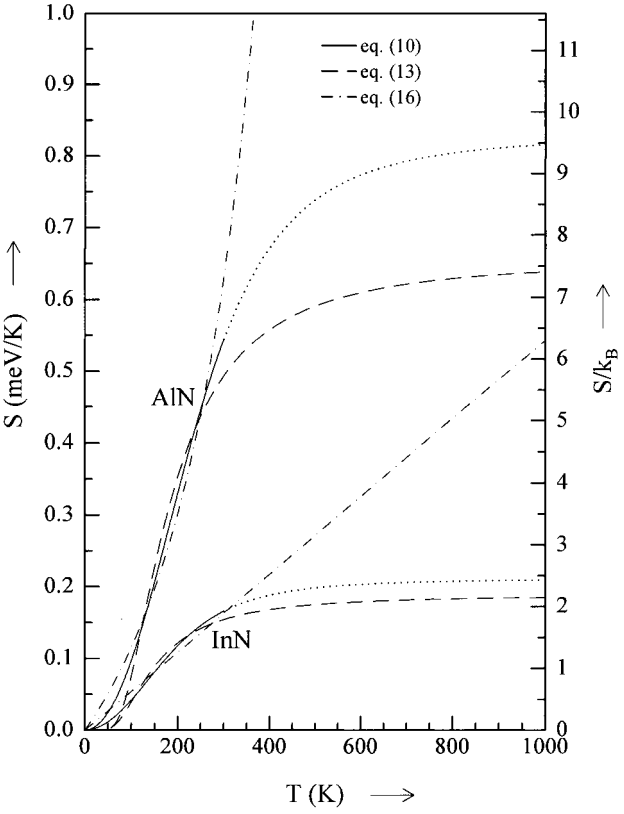


Fig. 17. Temperature dependencies of the slopes (2) associated with alternative fittings of the temperature dependencies of the gaps in AlN [16] (Fig. 5) and InN [26] (Fig. 10). The *concave* behavior of the $S_{\text{Var.}}(T)$ function (eq. (16)) in the case of AlN corresponds to the fitting regime with *negative* parameter sets, $\alpha_{\text{Var.}} < 0$ and $\beta < 0$ (cf. Section 5.3)

corresponds just to a *quadratic* $T$-dependence for the corresponding bandgap energy, i.e. simply

$$E(T) \to E(0) - cT^2 \,. \tag{18}$$

We have fitted the experimental data given for 15R SiC (Fig. 2) and for InN (Fig. 10) by eq. (18). The resulting parameter values are $E(0) = 2.988$ eV in combination with $c = 0.346 \times 10^{-6}$ eV/K$^2$, for 15R SiC, and $E(0) = 1.995$ eV in combination with $c = 0.272 \times 10^{-6}$ eV/K$^2$, for InN. These fits are represented by the dotted curves in Figs. 2 and 10. Comparing then Varshni's formula (4) with the quadratic dependence (eq. (18)) we see that the latter can be considered as a reduced version of Varshni's formula. This results readily from a limiting transition of both parameters to infinity ($\alpha_{\mathrm{Var.}} \to \pm\infty$ and $\beta \to \pm\infty$) under the restriction that the *ratio* between both parameters must tend just to the parameter $c$ in eq. (18), i.e.

$$c = \lim_{|\beta|\to\infty} \frac{\alpha_{\mathrm{Var.}}}{\beta} \,. \tag{19}$$

In fact, the apparently absurd parameter values $\alpha_{\mathrm{Var.}} = 17.5$ meV/K and $\beta = 50098$ K, which followed in Section 3.1 from an unbroken least-mean-square fitting of the data set for 15R SiC (Fig. 2) by eq. (4), give a ratio of $\alpha_{\mathrm{Var.}}/\beta = 0.351 \times 10^{-6}$ eV/K$^2$. This is almost the same as the magnitude of the parameter $c$ quoted above. Quite analogously, an unbroken fitting of the data set given by Guo and Yoshida [26] for InN (Fig. 10) by eq. (4) gives the parameter values $\alpha_{\mathrm{Var.}} = 444.6$ meV/K and $\beta = 1.637 \times 10^6$ K. Both values per se are absurd, again. But their ratio, $\alpha_{\mathrm{Var.}}/\beta = 0.272 \times 10^{-6}$ eV/K$^2$, is even perfectly coincident with the parameter $c$ given above for InN. These two cases of floating of Varshni's parameter set are a natural consequence of the absence of an inflection behavior of $S_{\mathrm{Var.}}(T)$ (eq. (16)). Such a floating of parameter values uses to occur in special cases where, owing to some critical $T_{\max}$ versus $T_{\mathrm{infl}}$ constellation, a minimum value for the variance can only be achieved within Varshni's model (eq. (4)) by adopting just a *linear* temperature dependence for the slope, $S_{\mathrm{Var.}}(T) \propto T$. In such a case, of course, a fitting procedure basing simply on the *quadratic* (*two*-parameter) model (18) for the gap energy is a priori more reasonable than a successive numerical approach via an order-of-magnitude floating of Varshni's parameters, because one obtains in this way immediately a finite value for the parameter $c$. In view of the direct connection of the latter with the curvature (second derivative) of the approximate $E(T)$ curve (eq. (18)), this parameter has at least some geometrical meaning. In contrast to this, the floating values of Varshni's parameters (i.e. $\alpha_{\mathrm{Var.}} \to \pm\infty$ and $\beta \to \pm\infty$ per se) have no meaning at all, neither a physical nor a geometrical one.

### *5.3 Changes of parameter signs*

We have plotted in Fig. 17 the $S(T)$ curve for AlN as following from eq. (10), with parameter values given in Table 1 . The corresponding inflection temperature follows from (12) to be relatively high in this case, $T_{\mathrm{infl}} \approx 180$ K. Comparing the latter with the experimental break-off temperature, $T_{\max} \approx 300$ K, we see that the characteristic temperature ratio is unusually low, $T_{\max}/T_{\mathrm{infl}} \approx 1.6$. Consequently, in contrast to all preceding examples discussed in Sections 5.1 and 5.2, the *concave* behavior of the $S(T)$ function is here largely *dominating* (cf. Fig. 17). Viewing the two qualitatively different patterns of the $\sigma_{\mathrm{Var.}}(\xi)$ function (16), which are plotted for $\xi > 0$ and $\xi < 0$ in Fig. 14, it is clear that

some numerical simulation of this predominantly concave behavior of the $S(T \leq 300\ \mathrm{K})$ curve for AlN can be achieved only by means of the latter alternative, i.e. $\xi \equiv T/\beta < 0$. This corresponds to some *negative* value for the parameter $\beta$. At the same time we see from eq. (16) (as well as from eq. (17)) that the parameter $\alpha_{\mathrm{Var.}}$ must adopt some *negative* value, too, in order to assure (at $\beta < 0$) the *positive* definiteness of the corresponding slope function, $S_{\mathrm{Var.}}(T) > 0$, within a range of $0 \leq T < |\beta|$ (i.e. *below* the corresponding singularity). Thus it is obvious that, within the frame of Varshni's model (eq. (4)), the actual minimum value for the variance can be approached only by starting the fitting procedure with *negative* values for *both* parameters, $\alpha_{\mathrm{Var.}}$ and $\beta$. In contrast to this, a start of the fitting procedure in the usual way, i.e. with positive values for both parameters, leads promptly to a floating of the parameter set, $\alpha_{\mathrm{Var.}} \to \infty$ and $\beta \to \infty$ (cf. Section 5.2). This means again an approach to a *quadratic* $E_{\mathrm{Var.}}(T)$ dependence (eq. (18)). In the case of AlN [16], a fit by the quadratic model (18) leads to a residual variance of $10\ \mathrm{meV}^2$ (with parameter values $E(0) = 6.202\ \mathrm{eV}$ and $c = 0.772 \times 10^{-6}\ \mathrm{eV/K}^2$). This is shown by the dotted curve in Fig. 5. In contrast to the latter, an unbroken least-mean-square procedure which has been started with a *negative* parameter set, $\alpha_{\mathrm{Var.}} < 0$ and $\beta < 0$, is ending at parameter values of $\alpha_{\mathrm{Var.}} = -0.34$ meV/K and $\beta = -736$ K. Apart from this physically absurd parameter constellation, the resulting $E_{\mathrm{Var.}}(T)$ curve provides a rather close approach to the observed $E(T)$ dependence (cf. the dash-dotted curve in the inset to Fig. 5). The corresponding variance of only about $0.94\ \mathrm{meV}^2$ shows that, from purely numerical points of view, the numerical simulation with negative parameter values is significantly better than that by the quadratic model (18) (cf. the dotted curve in the inset to Fig. 5). In this way we are concerned again with physically absurd parameter values indicating a break-down of Varshni's formula from physical points of view. This state of affairs, for AlN, is in analogy to results we have obtained by numerical analyses of another (less accurate) $E(T \leq 300\ \mathrm{K})$ data set given by Guo and Yoshida [26]. An unbroken fitting of the latter by Varshni's model (eq. (4)) led to a relaxed parameter constellation of $\alpha_{\mathrm{Var.}} = -0.165$ meV/K and $\beta = -445$ K.

An analogous situation is given also for the $E_{\mathrm{gx}}(T < 200\ \mathrm{K})$ data sets available for 4H SiC [42] and 6H SiC [43]. In both cases the break-off temperature is unusually low, $T_{\max} \approx 200$ K. (Note, in particular, that the latter is of the same order as $T_{\mathrm{infl}} = 217$ K estimated above for the case of 15R SiC.) This means that the concave parts of the $S(T)$ functions are again strongly dominating in both cases. Consequently, unrestricted least mean square procedures are tending to finite, negative parameter values. For the cases of 4H SiC [42] we have obtained $\alpha_{\mathrm{Var.}} = -0.441$ meV/K and $\beta = -342$ K. This is in analogy to the case of 6H SiC [43] where the corresponding parameter set is known from Varshni's paper [2] to be $\alpha_{\mathrm{Var.}} = -0.3055$ meV/K and $\beta = -311$ K. The corresponding (fictive) *singularities* are located in these cases at 342 and 311 K, respectively (i.e. but slightly above *room* temperature, which is physically obviously absurd).

These examples given here (and various others found in literature) suggest that an adoption of negative $\alpha_{\mathrm{Var.}}$ and $\beta$ values is by no means a rarity. This concerns in particular *wide* bandgap materials (like diamond, SiC, nitrides, etc.), as long as the experimentally chosen break-off temperatures are relatively low, $T_{\max} \lesssim 300$ K. Of course, the resulting negative parameter sets, $\alpha_{\mathrm{Var.}} < 0$ and $\beta < 0$, have absolutely no physical meaning. But, as demonstrated above (in Sections 5.1 and 5.2), even positive parameter sets of Varshni's type do not have a reasonable physical meaning.

## 6. Conclusions

In the present study we have performed detailed numerical analyses of the temperature dependencies of fundamental bandgap energies and exciton peak energy positions for a variety of group-IV, III–V, and II–VI semiconductor materials by a suitable *four*-parameter analytical model. By means of least square fits we have determined the corresponding material-specific sets of empirical parameters. For the sake of comparisons with more familiar *three*-parameter models (i.e. Varshni's formula and the Bose-Einstein-related model) we have also performed corresponding alternative fits for all materials in consideration. By comparing the residual variances characterizing the relative quality of alternative fits we have found that the four-parameter representation produced the *best* fits, for *all* materials in question. In addition to this we have found that the parameter values resulting from the fittings by this model are as a rule physically reasonable. Of especial importance are the reliable determinations of limiting slopes as a prerequisite for trustworthy extrapolations beyond the experimentally chosen break-off temperatures. A physically important by-product of these fittings by the four-parameter model are the estimations of material-specific dispersion ratios for most materials (which could in no way be estimated by simpler models). At the same time we have also shown that a use of Varshni's formula involves as a rule a significant overestimation of the limiting slope. Consequently, this formula is generally incapable of giving adequate results when it is used for extrapolations beyond the experimental break-off temperature. We have found that the principal analytical deficiency of Varshni's formula consists in its general incapability of simulating the characteristic *S-curve-like behavior* of the slopes of measured $E(T)$ curves. Such a behavior has been detected here for the majority of the materials in question. An estimation of the corresponding *inflection* temperatures for various *wide* bandgap materials has shown that they are located at much *higher* positions on temperature scale than usually found for conventional semiconductor materials (with bandgap energies <2 eV). This peculiar feature in combination with rather *high* magnitudes of Debye temperatures ($\Theta_D > 600$ K), the clearly *inadequate* analytical structure of Varshni's formula, and the usually *too low* positions of experimentally chosen break-off temperatures ($T_{max} \lesssim 300$ K) are the main reasons responsible for a large degree of *arbitrariness* of Varshni's parameter sets quoted in literature for GaN [54 to 59] and related materials.

***Acknowledgements*** The author would like to thank Dr. O. Ambacher, Walter Schottky Institute of the Technical University München, Germany, Dr. A. Parisini, Physical Department of the University of Parma, Italy, Dr. Qixin Guo, Department of Electrical and Electronic Engineering of the Toyohashi University of Technology, Toyohashi, Japan, Dr. H. Teisseyre, High Pressure Research Center of the Polish Academy of Sciences, Warsaw, Poland, and Dr. A. S. Zubrilov, Ioffe Physico-Technical Institute of the Russian Academy of Sciences, St. Peterburg, Russia, for having transmitted the $E(T)$ data published by their groups (Refs. [16], [25], [26], [47], and [48]) in digital form.

## References

[1] O. Madelung (ed.), Landolt-Börnstein: Numerical Data and Functional Relationships in Science and Technology, Group III, Vol. 17a and 22a, Springer-Verlag, Berlin 1982 and 1989.
[2] Y. P. Varshni, Physica **34**, 149 (1967).
[3] C. D. Thurmond, J. Electrochem. Soc. **122**, 1133 (1975).
[4] R. Pässler, J. Appl. Phys. **83**, 3356 (1998).

[5] L. VIÑA, S. LOGOTHETIDIS, and M. CARDONA, Phys. Rev. B **30**, 1979 (1984).
[6] K. P. O'DONNELL and X. CHEN, Appl. Phys. Lett. **58**, 2924 (1991).
[7] R. PÄSSLER, Solid-State Electronics **39**, 1311 (1996).
[8] R. PÄSSLER, phys. stat. sol. (b) **200**, 155 (1997).
[9] R. PÄSSLER, phys. stat. sol. (b) **193**, 135 (1996).
[10] C. D. CLARK, P. J. DEAN, and P. V. HARRIS, Proc. Roy. Soc. **A 277**, 312 (1964).
[11] L. PATRICK, D. R. HAMILTON, and W. J. CHOYKE, Phys. Rev. **132**, 2023 (1963).
[12] W. J. CHOYKE, Mater. Res. Bull. **4**, 141 (1969).
[13] W. BLUDAU, A. ONTON, and W. HEINKE, J. Appl. Phys. **45**, 1846 (1974).
[14] G. G. MACFARLANE, T. P. MCLEAN, J. E. QUARRINGTON, and V. ROBERTS, Phys. Rev. **111**, 1245 (1958).
[15] G. G. MACFARLANE, T. P. MCLEAN, J. E. QUARRINGTON, and V. ROBERTS, J. Phys. Chem. Solids **8**, 388 (1959).
[16] D. BRUNNER, H. ANGERER, E. BUSTARRET, F. FREUDENBERG, R. HÖPLER, R. DIMITROV, O. AMBACHER, and M. STUTZMANN, J. Appl. Phys. **82**, 5090 (1997).
[17] B. MONEMAR, SOLID STATE COMMUN. **8**, 1295 (1970).
[18] B. MONEMAR, Phys. Rev. B **8**, 5711 (1973).
[19] C. ALIBERT, A. JOULLIÉ, A. M. JOULLIÉ, and C. ANCE, Phys. Rev. **27**, 4946 (1983).
[20] H. HERR, Diplomarbeit, TU München, 1996.
[21] P. J. DEAN, G. KAMINSKY, and R. B. ZETTERSTROM, J. Appl. Phys. **38**, 3551 (1967).
[22] M. R. LORENZ, G. D. PETTIT, and R. C. TAYLOR, Phys. Rev. **171**, 876 (1968).
[23] E. GRILLI, M. GUZZI, R. ZAMBONI, and L. PAVESI, Phys. Rev. B **45**, 1638 (1992).
[24] M. B. PANISH and H. C. CASEY, JR., J. Appl. Phys. **40**, 163 (1969).
[25] C. GHEZZI, R. MAGNANINI, A. PARISINI, B. ROTELLI, L. TARRICONE, A. BOSACCHI, and S. FRANCHI, Phys. Rev. **52**, 1463 (1995).
[26] Q. GUO and A. YOSHIDA, Jpn. J. Appl. Phys. **33**, 2453 (1994).
[27] L. PAVESI, F. PIAZZA, A. RUDRA, J. F. CARLIN, and M. ILEGEMS, Phys. Rev. B **44**, 9052 (1991).
[28] Z. HANG, H. SHEN, and F. H. POLLAK, Solid State Commun. **73**, 15 (1990).
[29] Z. M. FANG, K. Y. MA, D. H. JAW, R. M. COHEN, and G. B. STRINGFELLOW, J. Appl. Phys. **67**, 7034 (1990).
[30] P. Y. LIU and J. C. MAAN, Phys. Rev. B **47**, 16274 (1993)
[31] R. PÄSSLER, E. GRIEBL, H. RIEPL, G. LAUTNER, S. BAUER, H. PREIS, W. GEBHARDT, B. BUDA, D. J. AS, D. SCHIKORA, K. LISCHKA, K. PAPAGELIS, and S. VES, J. Appl. Phys. **86**, 4403 (1999).
[32] R. PÄSSLER, F. BLASCHTA, E. GRIEBL, K. PAPAGELIS, B. HASERER, T. REISINGER, S. VES, and W. GEBHARDT, phys. stat. sol. (b) **204**, 685 (1997).
[33] D. G. SEILER, D. HEIMAN, R. FEIGENBLATT, R. L. AGGARWAL, and B. LAX, Phys. Rev. B **25**, 7666 (1982).
[34] D. G. THOMAS and J. J. HOPFIELD, Phys. Rev. **116**, 573 (1959).
[35] C. B. À LA GUILLAUME, J.-M. DEBEVER, and F. SALVAN, Phys. Rev. **177**, 567 (1969).
[36] A. ANEDDA and E. FORTIN, phys. stat. sol. (a) **36**, 385 (1976).
[37] S. LOGOTHETIDIS, M. CARDONA, P. LAUTENSCHLAGER, and M. GARRIGA, Phys. Rev. B **34**, 2458 (1986).
[38] J. P. LAURENTI, J. CAMASSEL, A. BOUHEMADOU, B. TOULOUSE, R. LEGROS, and A. LUSSON, J. Appl. Phys. **67**, 6454 (1990).
[39] K. A. DMITRENKO, L. V. TARANENKO, S. G. SHEVEL, and A. V. MARINTCHENKO, Fiz. Tekh. Poluprov. **19**, 788 (1985) [Soviet Phys. – Semicond. **19**, 487 (1985)].
[40] K. A. DMITRENKO, S. G. SHEVEL, L. V. TARANENKO, and A. V. MARINTCHENKO, phys. stat. sol. (b) **134**, 605 (1986).
[41] K.-C. CHIU, Y.-C. SU, and H.-A. TU, Jpn. J. Appl. Phys. **37** (Pt.1), 6374 (1998).
[42] W. J. CHOYKE, L. PATRICK, and D. R. HAMILTON, in: Proc. Internat. Conf. Physics of Semiconductors, Paris 1964, Dunod, Paris 1964 (p. 751).
[43] W. J. CHOYKE and L. PATRICK, Phys. Rev. **127**, 1868 (1962).
[44] W. J. CHOYKE, Mater. Res. Bull. **4**, 141 (1969).
[45] N. N. SIROTA and A. I. LUKOMSKII, Fiz. Tekh. Poluprov. **7**, 196 (1973) [Soviet Phys. – Semicond. **7**, 140 (1973)].
[46] J. C. NIPKO, C.-K. LOONG, C. M. BALKAS, and R. F. DAVIS, Appl. Phys. Lett. **73**, 34 (1998).
[47] H. TEISSEYRE, P. PERLIN, T. SUSKI, I. GRZEGORY, S. POROWSKI, J. JUN, A. PIETRASZKO, and T. D. MOUSTAKAS, J. Appl. Phys. **76**, 2429 (1994).

[48] A. S. Zubrilov, V. I. Nikolaev, D. V. Tsvetkov, V. A. Dmitriev, K. G. Irvine, J. A. Edmond, and C. H. Carter, Jr., Appl. Phys. Lett. **67**, 533 (1995).
[49] C. Lárez and C. Rincón, Mater. Lett. **24**, 211 (1995).
[50] P. R. Bevington and D. K. Robinson, Data Reduction and Error Analysis for the Physical Sciences, McGraw-Hill Inc., New York 1994.
[51] J. Aguilar-Hernández, G. Contreras-Puente, J. M. Figueroa-Estrada, and O. Zelaya-Angel, Jpn. J. Appl. Phys. **33**, 37 (1994).
[52] C. C. Kim, M. Daraselia, J. W. Garland, and S. Sivananthan, Phys. Rev. B **56**, 4786 (1997).
[53] H. Kim, G. Jeen, S. Park, Y.-H. Hwang, Y.-H. Um, and H. Park, Solid State Commun. **109**, 235 (1999).
[54] M. O. Manasreh, Phys. Rev. B **53**, 16425 (1996).
[55] L. Malikova, Y. S. Huang, F. H. Pollak, Z. C. Feng, M. Schurman, and R. A. Stall, Solid State Commun. **103**, 273 (1997).
[56] C. F. Li, Y. S. Huang, L. Malikova, and F. H. Pollak, Phys. Rev. B **55**, 9251 (1997).
[57] K. Kornitzer, K. Thonke, R. Sauer, M. Mayer, M. Kamp, and K. J. Ebeling, J. Appl. Phys. **83**, 4397 (1998).
[58] A. K. Viswanath, J. I. Lee, S. Yu, D. Kim, Y. Choi, and C.-H. Hong, J. Appl. Phys. **84**, 3848 (1998).
[59] A. K. Viswanath, J. I. Lee, C. R. Lee, J. Y. Leem, and D. Kim, Solid State Commun. **108**, 483 (1998).